発表者氏名	論文タイトル名	発表誌名	巻号	ページ	出版年
Ikeya S, Urano S, Tokura Y.	Linear IgA bullous dermatosis following human papillomavirus vaccination.	Eur J Dermatol.	[in press]		
Ito T, Shimomura Y, Ogai M, Sakabe J-I, Tokura Y.	Identification of a novel heterozygous mutation in the first Japanese case of Marie Unna hereditary hypotrichosis.	J Dermatol.	[in press]		
Shiraishi Y, Jia Y, Domenico J, Joetham A, Karasuyama H, Takeda K, and Gelfand E.W.	Sequential engagement of FcεRI on mast cells and basophil histamine H4 receptor and FcεRI in allergic rhinitis.	J. Immunol.	[in press]		
坂部純一，黒田悦史，戸倉新樹	PI3 キナーゼ経路による好塩基球における Th2 サイトカインの産生制御	臨床免疫・アレルギー科	56	622-627	2011
池谷茂樹，浦野聖子，小出まさよ，戸倉新樹	顕著な炎症を伴った汗孔角化症	皮膚病診療	33	813-816	2011
澤田雄宇，戸倉新樹	成人Ｔ細胞性白血病／リンパ腫皮疹型と予後判定への重要性	日本皮膚科学会雑誌	121	3091-3093	2011
安東嗣修，倉石　泰	温清飲による痒みの抑制機序	phil 漢方	40	26-28	2012
壱岐美紗子, 烏山　一	好塩基球研究の進展	医学のあゆみ	243(1)	78-83	2012
鬼頭由紀子，笹田久美子，八木宏明，大島昭博，戸倉新樹	アトピー性皮膚炎との鑑別を要した若年発症ＳｅＺａｒｙ症候群	Visual Dermatology	11	912-914	2012
吉木竜太郎，中村元信，戸倉新樹	紫外線による皮膚における免疫抑制とその役割	J UOEH（産業医科大学雑誌）	34	77-83	2012
戸倉新樹	Bowen 病と好酸球性膿疱性毛包炎	皮膚科の臨床	54	7-12	2012
戸倉新樹	低悪性度 T 細胞性リンパ腫に対する薬物療法-菌状息肉症	臨床腫瘍プラクティス	8	258-261	2012
戸倉新樹	皮膚バリアからみるアトピー性皮膚炎の全体像	臨床免疫・アレルギー科	58	295-299	2012
戸倉新樹	Th17 細胞と皮膚疾患	日本臨床免疫学会会誌	35	388-392	2012
戸倉新樹	IgE 値正常の内因性アトピー性皮膚炎の成因は如何に	皮膚アレルギーフロンティア	10	19-23	2012
戸倉新樹，小林美和	掌蹠膿疱症の治療／ロキシスマイシン内服療法	Visual Dermatology	11	1071-1072	2012
戸倉新樹，澤田雄宇，島内隆寿	成人Ｔ細胞性白血病／リンパ腫（adlt T-cell leukemia/lymphoma：ATLL）	Visual Dermatology	11	940-945	2012
江川真由美, 烏山　一	好塩基球研究のアップデート	実験医学	30(6)	905-911	2012
佐藤孝浩，横関博雄，片山一朗，室田浩之，戸倉新樹，朴紀央，椛島健治，中溝 聡，高森建二，塩原哲夫，三橋善比古，森田栄伸	慢性痒疹診療ガイドライン	日本皮膚科学会雑誌	122	1-16	2012

発表者氏名	論文タイトル名	発表誌名	巻号	ページ	出版年
坂部純一，秦 まき，平川聡史，戸倉新樹	PCR 法による単純および帯状疱疹ウイルス感染症の迅速診断：成人および小児例	日小皮会誌	31	47-50	2012
菅谷誠，河井一浩，大塚幹夫，濱田利久，米倉健太郎，島内隆寿，谷 守，古賀弘志，野崎浩二，伊豆津宏二，戸倉新樹，瀬戸山充，長谷哲男，岩月啓氏	皮膚リンパ腫診療ガイドライン２０１１年改訂版	日本皮膚科学会雑誌	122	1513-1531	2012
大日輝記，川口淳，上田説子，内小保理，占部和敬，小林美和，下田貴子，十亀良介，高守史子，田中倫子，寺原慶子，中園亜矢子，文森健明，師井美樹，山本有紀，渡邉徹心，須賀康，古江増隆，戸倉新樹，川名誠司，古川福実，山元修，橋本 隆	サリチル酸マクロゴーグルピーリングによる尋常性痤瘡の治療効果 -多施設無作為化二重盲検ハーフサイド対照比較試験-	Aesthetic Dermatology（日本美容皮膚科学会雑誌）	22	31-39	2012
中島沙恵子，椛島健治	Langerhans 細胞への TSLP の作用とアトピー性皮膚炎	臨床免疫・アレルギー科	58(3)	334-340	2012
田村愛子，冨田浩一，鈴木陽子，戸倉新樹	小児の顔面に生じた Mycobacterium chelonae 感染症の１例	日小皮会誌	31	59-61	2012
島内隆寿，戸倉新樹	感染性肉芽腫との鑑別を要した肉芽腫性菌状息肉症	Visual Dermatology	11	922-923	2012
鈴木健晋，鈴木陽子，冨田洋一，平川聡史，戸倉新樹	Osler 病との鑑別を要した抗セントロメア抗体高値陽性の多発毛細血管拡張	皮膚病診療	34	481-484	2012
中島沙恵子，椛島健治	マスターレギュレーターとしての TSLP	Modern Physician	33(2)	198-202	2013

1521-0103/12/3431-91–96$25.00
THE JOURNAL OF PHARMACOLOGY AND EXPERIMENTAL THERAPEUTICS
Copyright © 2012 by The American Society for Pharmacology and Experimental Therapeutics
JPET 343:91–96, 2012

Vol. 343, No. 1
195222/3793408

Involvement of Serine Protease and Proteinase-Activated Receptor 2 in Dermatophyte-Associated Itch in Mice

Tsugunobu Andoh, Yusuke Takayama, Takako Yamakoshi, Jung-Bum Lee, Ayako Sano, Tadamichi Shimizu, and Yasushi Kuraishi

Departments of Applied Pharmacology (T.A., Y.T., Y.K.), Dermatology (T.Y., T.S.), and Pharmacognosy (J.-B.L.), Graduate School of Medicine and Pharmaceutical Sciences, University of Toyama, Toyama, Japan; and Graduate School of Agriculture, University of the Ryukyu, Okinawa, Japan (A.S.)

Received April 4, 2012; accepted July 2, 2012

ABSTRACT

We investigated the involvement of serine protease and proteinase-activated receptor 2 (PAR_2) in dermatophyte-induced itch in mice. An intradermal injection of an extract of the dermatophyte *Arthroderma vanbreuseghemii* (ADV) induced hind-paw scratching, an itch-related behavior. ADV extract-induced scratching was inhibited by the opioid receptor antagonists naloxone and naltrexone, the serine protease inhibitor nafamostat mesylate, and the PAR_2 receptor antagonist FSLLRY-NH_2. ADV extract-induced scratching was not inhibited by the H_1 histamine receptor antagonist terfenadine or by mast cell deficiency. Heat pretreatment of the ADV extract markedly reduced the scratch-inducing and serine protease activities. Proteolytic cleavage within the extracellular N terminus of the PAR_2 receptor exposes a sequence that serves as a tethered ligand for the receptor. The ADV extract as well as tryptase and trypsin cleaved a synthetic N-terminal peptide of the PAR_2 receptor. The present results suggest that serine protease secreted by dermatophytes causes itching through activation of the PAR_2 receptors, which may be a causal mechanism of dernatophytosis itch.

Introduction

Superficial cutaneous fungal infections, especially tinea, are very common in dermatological foot diseases, and cause skin conditions, such as scales, keratosis, erosion, and itching; itching is reported by approximately 50% of patients with tinea pedis (Cohen et al., 2002; Djeridane et al., 2006). Fungi proteinase has long been known to be pruritogenic in humans (Arthur and Shelley, 1955). Dermatophyte infection leads to immediate and delayed-type hypersensitivities (Woodfolk, 2005), which can cause pruritus. However, the details of the underlying mechanisms of dermatophytosis pruritus remain poorly understood. Dermatophytes secrete a variety of enzymes, such as proteases, lipases, elastases, collagenases, phosphatases, and esterases, which are important factors during the infection process (Peres et al., 2010). Therefore, we first aimed to determine whether dermatophyte products, especially proteases, cause acute itching.

Proteases have long been known to cause itching in humans; moreover, endopeptidases rather than exopeptidases cause itching (Arthur and Shelley, 1955). Among the endopeptidases (proteinases), serine proteases may cause itching via proteinase-activated receptor (PAR), a family member of the G-protein-coupled receptors. The activation of PAR is initiated by the cleavage of the N terminus of the receptor to generate a new tethered ligand terminus, which activates PAR itself (Macfarlane et al., 2001). The PAR_1, PAR_3, and PAR_4 receptor subtypes are thrombin receptors, whereas PAR_2 is activated by trypsin-type serine proteases rather than by thrombin (Macfarlane et al., 2001). Trypsin-type serine proteases and a synthetic PAR_2 tethered ligand cause itching and scratching in humans and animals (Steinhoff et al., 2003; Shimada et al., 2006; Ui et al., 2006; Tsujii et al., 2009). However, PAR_1 and PAR_4 tethered ligands elicit mild scratching, which is inhibited by the H_1 histamine receptor antagonist terfenadine in mice (Tsujii et al., 2008). Chymase, a chymotrypsin-type serine protease, causes itching in humans, probably by degranulating mast cells (Hagermark et al., 1972). Therefore, the second aim of this study was to determine whether the PAR_2 receptor and mast cell degran-

This work was supported in part by the Ministry of Education, Culture, Sports, Science and Technology, Japan [Grants-in-Aid for Young Scientists (B) 19790051, 22790063]; the Ministry of Education, Culture, Sports, Science and Technology, Japan [Grant-in-Aid for Scientific Research (B)23390153]; and the Health, Labor and Welfare Ministry, Japan. This work was also supported in part by the National BioResource Project in Japan (http://www.nbrp.jp/).

Article, publication date, and citation information can be found at http://jpet.aspetjournals.org.
http://dx.doi.org/10.1124/jpet.112.195222.

ABBREVIATIONS: PAR, proteinase-activated receptor; ADV, *A. vanbreuseghemii*; FK888, N^2-[(4*R*)-4-hydroxy-1-(1-methyl-1*H*-indol-3-yl)carbonyl-L-prolyl]-*N*-methyl-*N*-phenylmethyl-3-(2-naphthyl)-L-alaninamide.

ulation are involved in the itching induced by dermatophyte products.

Materials and Methods

Animals. Male ICR mice (5–9 weeks old or neonatal) were used, with the exception of one series of experiments in which male mast cell-deficient mice (WBB6F1 W/W^v) and the normal littermates [WBB6F1(+/+)] were used at 8 weeks of age. All mice were purchased from Japan SLC (Shizuoka, Japan). The mice were housed in a room under controlled temperature (21–23°C), humidity (45–65%), and light (lights on from 7:00 AM to 7:00 PM). Food and water were made freely available. Procedures in the animal experiments were approved by the Committee for Animal Experiments at University of Toyama and were conducted in accordance with the guidelines of the Japanese Pharmacological Society.

Materials. Naloxone hydrochloride and naltrexone hydrochloride (both from Sigma-Aldrich, St. Louis, MO) were dissolved in physiological saline and injected subcutaneously 15 min before dermatophyte extract injection. Terfenadine (Sigma-Aldrich) was dissolved in 0.5% sodium carboxymethyl cellulose (Wako Pure Chemical Industries, Osaka, Japan) and administered orally 30 min before *Arthroderma vanbreuseghemii* (ADV) extract injection. Nafamostat mesylate (Torii Pharmaceutical Co., Ltd., Tokyo, Japan) was dissolved in 5% glucose (Wako Pure Chemical Industries) and injected intravenously 5 min before ADV extract injection. The peptides FSLLRY-NH_2, SLIGRL-NH_2, LRGILS-NH_2, GRNNSKGRSLIGRLET-NH_2, and GRNNSKGIILIGRLET-NH_2 were synthesized and identified using the peptide synthesizer PSSM-8 (Shimazu Co., Kyoto, Japan) and matrix-assisted laser desorption/ionization time-of-flight mass spectrometer Autoflex T1 (Bruker Daltonics, Billerica, MA), respectively. FSLLRY-NH_2 was dissolved in physiological saline (Ohtsuka Pharmaceutical Co., Ltd., Tokushima, Japan) and injected intradermally together with ADV extract. *N*-p-Tosyl-Gly-Pro-Arg *p*-nitroanilide was purchased from Sigma-Aldrich, and tryptase and trypsin were from Wako Pure Chemical Industries.

Dermatophytes and Extract Preparation. The dermatophyte ADV was obtained from the National BioResource Project (http://www.nbrp.jp/). It was subcultured on 2% agar (Wako Pure Chemical Industries) containing potato dextrose broth (Wako Pure Chemical Industries) at room temperature. A colony containing fungal spores was removed, added to Sabouraud dextrose liquid culture medium containing 2% dextrose (Wako Pure Chemical Industries) and 1% polypeptone (Wako Pure Chemical Industries), and incubated at 37°C for more than 3 days.

The colonies of ADV were repeatedly washed with physiological saline and centrifuged until the supernatant became transparent. The resultant pellet was suspended in physiological saline and subjected to repeated freeze-thaw cycles and sonication. After centrifugation, the supernatant (ADV extract) was collected and concentrated using a centrifugal concentrator Vivaspin 20 with a molecular mass cutoff of 30 kDa (Vivascience AG, Hannover, Germany). The protein concentration was determined using a protein assay kit (Bio-Rad, Hercules, CA). In a series of experiments, ADV extract that was heat-treated at 100°C for 1 h was used.

Behavioral Experiments. The day before the experiments were conducted, hair was removed from the rostral part of the back or the unilateral cheek of the mice using hair clippers. The animals were put individually in an acrylic cage composed of four cells (13 × 9 × 35 cm) for at least 1 h for acclimation. Intradermal injection was administered in a volume of 50 μl to the rostral back and 20 μl to the cheek. Immediately after intradermal injection, the animals were returned to the same cells, and their behaviors were videotaped for 1 h; no personnel were present in the observation room during this time. Playback of the video served for determination of hind-paw scratching of the rostral back or cheek and forelimb wiping of the cheek (Kuraishi et al., 1995; Shimada and LaMotte, 2008). When mice scratch, they stretch the hind paw toward the treated site, lean the head toward the hind paw, rapidly move the paw several times, and then lower it back to the floor; a series of these movements was counted as one bout of scratching (Andoh et al., 2004).

Determination of Trypsin-Like Serine Proteinase Activity. *N*-p-Tosyl-Gly-Pro-Arg *p*-nitroanilide acetate (Sigma-Aldrich), a substrate for trypsin-like serine proteases, was dissolved in 50 mM Tris-HCl, pH 8.0, in a concentration of 0.5 mg/ml. A 0.02-ml volume of ADV extract or heat-treated ADV extract was added to 0.18 ml of the substrate solution, and the mixture was incubated at 37°C for 1 h. The amount of *p*-nitroanilide released was colorimetrically determined at 420 nm.

Activity of PAR_2 Cleavage. Ten micrograms of GRNNSKGRSLIGRLET-NH_2 (an N-terminal peptide of PAR_2 containing a tethered ligand sequence SLIGRL) and its analog GRNNSKGIILIGRLET-NH_2 (two amino acids, Arg-Ser, of trypsin-like serine protease-cleaved site were replaced by Ile-Ile) were reacted with ADV extract (10-μg protein), tryptase (1 μg), or trypsin (1 μg) in 50 mM Tris-HCl, pH 8.0, in a volume of 100 μl for 1 h. After adding a dye, the reaction mixture was electrophoresed on a 20% SDS-polyacrylamide gel (Wako Pure Chemical Industries). Because the reaction product was too small to be separated by electrophoresis, the gel

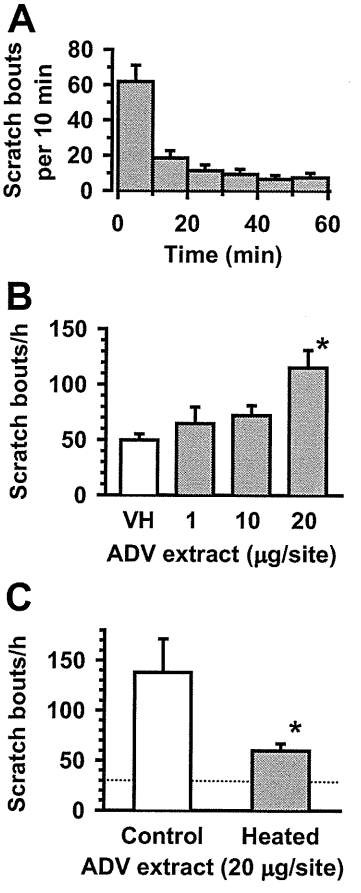

Fig. 1. Scratching response to intradermal injection of dermatophyte extract into the back in ICR mice. Mice were administered an intradermal injection of an extract of the dermatophyte ADV or vehicle (VH). A, time course of scratching after ADV extract (20 μg/site) injection. B, dose-response curve for the scratch-inducing effect of ADV extract. Values represent the means ± S.E.M. for 8 to 14 animals. *, $P < 0.05$ compared with VH (Dunnett's multiple comparisons). C, effect of heat treatment on the scratch-inducing activity of ADV extract. Heat-treated and untreated ADV extracts were injected intradermally at a dose of 20 μg/site. The dotted line represents the average value of the VH-injected group. Values represent the means ± S.E.M. for seven to eight animals. *, $P < 0.05$ (Student's *t* test).

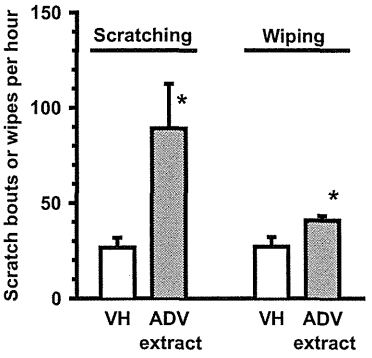

Fig. 2. Scratching and wiping responses to intradermal injection of dermatophyte extract into the cheek in ICR mice. Mice were administered an intradermal injection of ADV extract (20 μg/site) or VH, and scratching bouts and wiping actions of each mouse were counted for 1 h. Values represent the means ± S.E.M. for six animals. *, $P < 0.05$ (Student's t test).

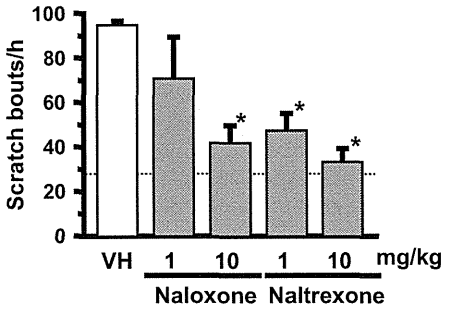

Fig. 3. Effects of opioid receptor antagonists on scratching responses to intradermal injection of dermatophyte extract into the back in ICR mice. Mice were administered an intradermal injection of ADV extract (20 μg/site), and scratching bouts were counted for 1 h. The opioid antagonist naloxone hydrochloride, μ-opioid receptor antagonist naltrexone hydrochloride, and vehicle (VH) were injected subcutaneously 15 min before ADV extract injection. The dotted line represents the average value of scratching bouts in mice given intradermal injection of saline. Values represent the means ± S.E.M. for six animals. *, $P < 0.05$ compared with VH (Dunnett's multiple comparisons).

was stained with Coomassie Brilliant Blue (Wako Pure Chemical Industries), and the substrate peptide was determined.

Data Processing. Data are presented as means ± S.E.M. Statistical significance was analyzed using Dunnett's multiple comparisons, Bonferroni's multiple comparisons, or Student's t test; $P < 0.05$ was considered significant.

Results

Behavioral Effects of Dermatophyte Extract. *Trichophyton mentagrophytes* is a common dermatophyte isolated from humans (Seebacher et al., 2008), and ADV, which belongs to the *T. mentagrophytes* complex, infects animals and humans (Drouot et al., 2009). Therefore, we examined the pruritogenic activity of an extract prepared from cultured ADV. When injected intradermally into the rostral back of mice, ADV extract elicited hind-paw scratching—an itch-related behavior—of the injection site at a dose of 20 μg/site; the effect peaked during the first 10-min period and almost subsided by 40 min (Fig. 1A). Scratching was dose-dependently increased in the range of 1 to 20 μg of ADV extract per injection site; significant increase was observed at the dose of 20 μg/site (Fig. 1B). Heat treatment of the ADV extract almost abolished its scratch-eliciting activity (Fig. 1C).

We also injected ADV extract into the murine cheek to test whether the extract is algogenic. Forelimb wiping—a nociceptive behavior—was slightly but significantly increased by ADV extract (20 μg/site) compared with the vehicle, whereas hind-paw scratching was markedly increased in the same individuals (Fig. 2); the increases in scratching elicited from injection into the cheek were similar to those from injection into the rostral back (Figs. 1B and 2).

Effects of Various Agents on ADV Extract-Induced Scratching. Subcutaneous pretreatment with the opioid receptor antagonist naloxone hydrochloride (1 and 10 mg/kg) and selective μ-opioid receptor antagonist naltrexone hydrochloride (1 and 10 mg/kg) inhibited ADV extract-induced scratching in a dose-dependent manner (Fig. 3). Oral pretreatment with 30 mg/kg H_1 histamine receptor antagonist terfenadine had no effect (Fig. 4A). Intravenous pretreatment with the serine proteinase inhibitor nafamostat mesylate (1–10 mg/kg) inhibited ADV extract-induced scratching;

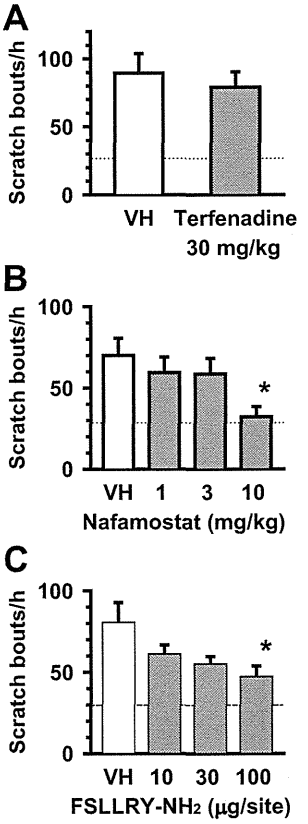

Fig. 4. Effects of H_1 histamine receptor antagonist, serine protease inhibitor, and PAR_2 antagonist on scratching responses to intradermal injection of dermatophyte extract into the back in ICR mice. Mice were administered an intradermal injection of ADV extract (20 μg/site), and scratching bouts were counted for 1 h. A, terfenadine (30 mg/kg) and VH were administered orally 30 min before ADV extract injection. B, nafamostat mesilate and vehicle (VH) were injected intravenously 5 min before ADV extract injection. C, FSLLRY-NH_2 and VH were injected intradermally together with ADV extract. Dotted lines represent the average value of scratching bouts in mice given intradermal injection of saline. Values represent the means ± S.E.M. for six animals. *, $P < 0.05$ compared with VH (Student's t test or Dunnett's multiple comparisons).

significant inhibition was observed at a dose of 10 mg/kg (Fig. 4B). Simultaneous local treatment with the PAR_2 receptor antagonist FSLLRY-NH_2 (10–100 μg/site) inhibited ADV extract-induced scratching, with a significant inhibition observed at a dose of 100 μg/site (Fig. 4C).

Effect of Mast Cell Deficiency on ADV Extract-Induced Scratching. An intradermal injection of ADV extract (20 μg/site) significantly increased scratching in mast cell-deficient mice (WBB6F1 *W/W*^{v}) and in normal littermates [WBB6F1(+/+)], compared with saline-injected group (Fig. 5). The extent of ADV extract-induced scratching was similar in these mice (Fig. 5). An intradermal injection of the PAR_2 receptor agonist SLIGRL-NH_2 (50 nmol/site) also significantly increased in WBB6F1 *W/W*^{v} and WBB6F1(+/+) mice, compared with negative control (50 nmol/site of the reverse peptide LRGILS-NH_2); the extent of SLIGRL-NH_2-induced scratching was similar in these mice (Fig. 6).

Trypsin-Like Serine Proteinase Activity of ADV Extract. The ADV extract (0.5–100 μg/ml) showed serine protease activity in a concentration-dependent manner (Fig. 7). Heat treatment markedly decreased the proteinase activity of the ADV extract with traces of activity remaining (Fig. 7).

Cleavage of N-terminal Peptide of PAR_2 Receptor by ADV Extract. Proteolytic cleavage within the extracellular N terminus of PAR_2 receptor exposes a receptor-activating N-terminal sequence that serves as a tethered ligand for the receptor (Macfarlane et al., 2001). A synthetic N-terminal peptide of PAR_2 receptor, GRNNSKGRSLIGRLET-NH_2, was cleaved by the ADV extract as well as by tryptase and trypsin; thus, it disappeared from the reaction mixture after a 1-h reaction (Fig. 8A). In contrast, tryptase did not cleave the analog peptide GRNNSKGIILIGRLET-NH_2 (Fig. 8B). ADV extract decreased the analog peptide, but 63% remained after a 1-h reaction (Fig. 8B).

Discussion

Intradermal injections of ADV extract into the rostral back and cheek induced hind-paw scratching in mice, and its injection into the cheek elicited only slight wiping. Intradermal injections of pruritogenic and algogenic substances (such as histamine and capsaicin, respectively) into the cheek have been shown to elicit hind-paw scratching and forelimb wiping, respectively, of the injection site in mice (Shimada and LaMotte, 2008). Therefore, the present results suggest that the ADV extract is more pruritogenic and less algogenic.

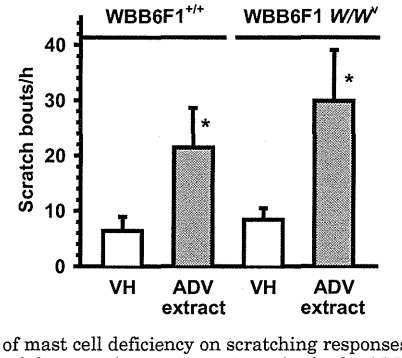

Fig. 5. Effect of mast cell deficiency on scratching responses to intradermal injection of dermatophyte extract into the back. ADV extract (20 μg/site) and vehicle (VH) were injected intradermally in mast cell-deficient WBB6F1 *W/W*^{v} mice and in normal littermates (WBB6F1$^{+/+}$). Scratching bouts were counted for 1 h after intradermal injection. Values represent the means ± S.E.M. for seven (ADV extract) or eight (VH) animals. *, $P < 0.05$ compared with the corresponding VH (Bonferroni's multiple comparisons).

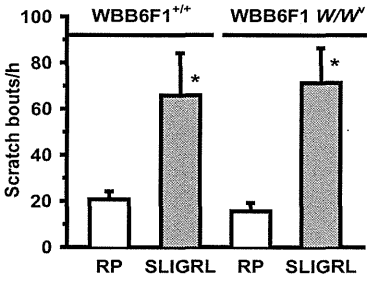

Fig. 6. Scratch-inducing effect of PAR_2 receptor agonist peptide in WBB6F1 mice. The PAR_2 receptor agonist peptide SLIGRL-NH_2 (SLIGRL) and the reverse peptide (RP) LRGILS-NH_2 were injected intradermally at a dose of 50 nmol/site in mast cell-deficient WBB6F1 *W/W*^{v} mice and in normal littermates (WBB6F1$^{+/+}$). Scratching bouts were counted for 1 h after intradermal injection. Values represent the means ± S.E.M. for seven (SLIGRL) or eight (RP) animals. *, $P < 0.05$ compared with the corresponding RP (Bonferroni's multiple comparisons).

Itch-related, but not pain-related, behaviors are suppressed by opioid receptor antagonists (Akiyama et al., 2010; Gotoh et al., 2011). Opioid receptor antagonists have been shown to inhibit the scratching induced by several pruritogens (Andoh et al., 1998, 2009; Yamaguchi et al., 1999), dermatoses in rodents (Ohtsuka et al., 2001; Yamaguchi et al., 2001; Miyamoto et al., 2002), and pruritus in humans with pruritic diseases (Monroe, 1989; Bergasa et al., 1995). Opioid receptor antagonists exert antipruritic activity via the action on μ-opioid receptors in the central nervous system (Maekawa et al., 2002; Nojima et al., 2003), especially in the lower brainstem (Kuraishi et al., 2008). Thus, the result that the scratching induced by ADV extract injection into the rostral back was suppressed by opioid receptor antagonists supports the idea that ADV extract was primarily pruritogenic in the skin.

ADV extract-induced scratching was not inhibited by the H_1 histamine receptor antagonist terfenadine, even at a dose that almost completely inhibits both histamine-induced scratching (Ohtsuka et al., 2001) and immediate allergy-induced plasma extravasation (Ohtsuka et al., 2001; Andoh

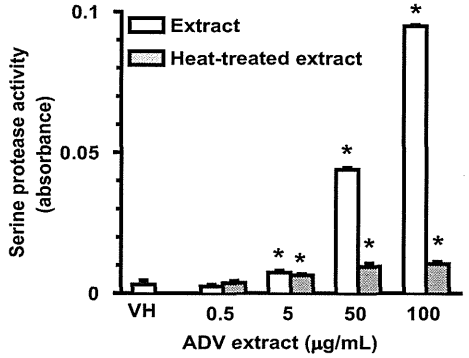

Fig. 7. Trypsin-like serine protease activity in the dermatophyte extract. ADV extract with or without prior heat treatment were added to the solution of *N*-p-Tosyl-Gly-Pro-Arg *p*-nitroanilide, a substrate for trypsin-like serine proteases. The amount of *p*-nitroanilide released was colorimetrically determined. Values represent the means ± S.E.M. for eight samples. *, $P < 0.05$ compared with VH (Dunnett's multiple comparisons).

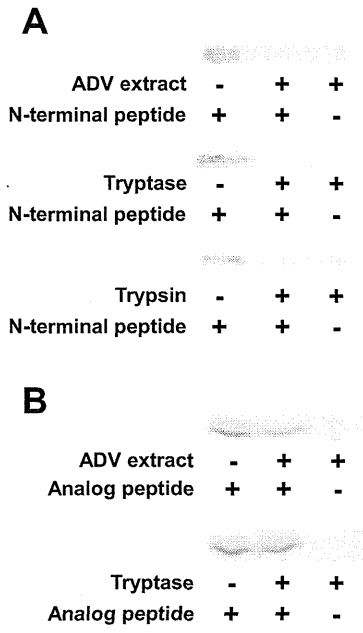

Fig. 8. Cleavage of N-terminal peptide of the PAR_2 receptor with dermatophyte extract, tryptase, and trypsin. A, GRNNSKGRSLIGRLET-NH_2 (N-terminal peptide of PAR_2 containing protease-cleaved sequence) and B, its analog GRNNSKGIILIGRLET-NH_2 (two amino acids of trypsin-like serine protease-cleaved site were replaced) were reacted with ADV extract (10 μg), tryptase (1 μg), or trypsin (10 μg) in a volume of 100 μl for 1 h. After adding the dye solution (25 μl), the reaction mixtures were applied in a volume of 30 μl per lane. The signal of the band was determined with Coomassie Brilliant Blue. These experiments were repeated three times, and provided similar results.

et al., 2010). In addition, ADV extract elicited scratching to a similar extent in both mast cell-deficient mice and normal littermates. Therefore, it is suggested that histamine and mast cell degranulation are not the main causes of ADV-induced scratching.

The ADV extract had serine protease activity and its scratch-inducing activity was suppressed by nafamostat mesylate, a serine protease inhibitor (Mori et al., 2003). The dose response of the anti-ADV effect of nafamostat was similar to that of its effect on scratching induced by intradermal injection of the serine protease tryptase in mice (Ui et al., 2006). Taken together, these results suggest that serine proteases are involved in ADV extract-induced itching. The results that heat treatment of the ADV extract markedly decreased its scratch-inducing and serine protease activities support the above-mentioned idea. Dermatophytes require keratin for growth and generally invade only superficial keratinized structures (Vermout et al., 2008). Dermatophytes secrete endoproteases and exoproteases of 30 to 50 kDa (Monod, 2008). Although pruritogenic proteases have not been identified, one possible protease secreted by the dermatophytes is keratinase. Keratinase is a serine protease (Meevootisom and Niederpruem, 1979; Gradisar et al., 2000), which is secreted from dermatophytes (Yu et al., 1968; Muhsin and Salih, 2001; Monod, 2008), and catalyzes the degradation of the keratin present in the host tissue into oligopeptides (Peres et al., 2010). In preliminary experiments, the ADV extract had keratinase activity, and an intradermal injection of keratinase purified from *Bacillus licheniformis* induced scratching in mice (T. Andoh, Y. Takayama, and Y. Kuraishi, unpublished observation). Thus, dermatophyte keratinase may be pruritogenic, but we do not deny the possibility that the other dermatophyte proteases are also pruritogenic.

PAR_2 receptor is activated via the proteolytic cleavage of its N-terminal sequence by serine proteases (Macfarlane et al., 2001). In the present study, the ADV extract as well as tryptase and trypsin cleaved the N-terminal peptide of PAR_2 receptor, suggesting that the ADV extract has PAR_2-stimulating activity. The PAR_2 receptor antagonist FSLLRY-NH_2 (Al-Ani et al., 2002) inhibited the ADV extract-induced scratching. The dose response of the anti-ADV effect of FSLLRY-NH_2 was similar to that of its effect on scratching induced by intradermal tryptase in mice (Ui et al., 2006). Thus, it is suggested that the ADV extract caused scratching via the activation of PAR_2 receptors. The activation of PAR_1 and PAR_4 also causes scratching, at least partly through the release of histamine from mast cells (Tsujii et al., 2008). However, as mentioned above, histamine and mast cells did not play essential roles in the scratch-inducing activity of ADV extract, and PAR_1 and PAR_4 receptors may not be involved in the ADV action. Tryptase almost completely cleaved an N-terminal peptide of PAR_2 receptor, GRNNSK-GRSLIGRLET-NH_2, but not the analog GRNNSKGIILI-GRLET-NH_2, suggesting that the analog peptide is resistant to trypsin-like serine protease. The ADV extract almost completely or partly cleaved the N-terminal peptide of PAR_2 receptor or the analog, suggesting that although the ADV extract has mainly trypsin-like serine protease activity, it also has other protease activity. It is unknown whether non-trypsin like protease activity is involved in the scratch-inducing action of the ADV extract.

Because dermatophytes generally invade only keratinized structures, the epidermis may be a causative site for dermatophytosis pruritus. The PAR_2 receptors are present in a high density in epidermal keratinocytes (Steinhoff et al., 2003; Tsujii et al., 2009), except in the basal layer (Tsujii et al., 2009). Keratinocytes release several itch mediators and itch enhancers, such as leukotriene B_4 (Andoh and Kuraishi, 1998; Andoh et al., 2001, 2004, 2009), thromboxane A_2 (Andoh et al., 2007), and nitric oxide (Andoh and Kuraishi, 2003). Recently, it has been shown that leukotriene B_4 is produced in cultured keratinocytes by stimulation of PAR_2 receptors and that intradermal PAR_2 agonist-induced scratching is suppressed by a 5-lipoxygenase inhibitor in mice (Zhu et al., 2009). These findings taken together raise the possibility that serine proteases secreted by dermatophytes activate PAR_2 receptors in the epidermal keratinocytes to secrete itch mediators including leukotriene B_4.

PAR_2 receptors are also present in nerve fibers in the human skin (Steinhoff et al., 2003). In rodents, PAR_2 receptors are expressed in neurons in the dorsal root ganglion, and some PAR_2-positive neurons contain neuropeptides such as substance P and calcitonin gene-related peptide (Steinhoff et al., 2000). It has been reported that intradermal trypsin-induced scratching is mediated by substance P release and mast cell degranulation, namely mediated by a neurogenic inflammatory mechanism, in mice (Costa et al., 2008). However, in the present study, an intradermal injection of ADV extract increased scratching in both mast cell-deficient mice and normal littermates, thus, excluding the contribution of mast cell in the response. In addition, an intradermal injec-

tion of PAR_2 receptor agonist peptide increased scratching in both mast cell-deficient mice and normal littermates; the extent of scratching was similar to that in ICR mice (Tsujii et al., 2008). In preliminary experiments, the NK_1 tachykinin receptor antagonists spantide N^2-[(4*R*)-4-hydroxy-1-(1-methyl-1*H*-indol-3-yl)carbonyl-L-prolyl]-*N*-methyl-*N*-phenylmethyl-3-(2-naphthyl)-L-alaninamide (FK888) (Fujii et al., 1992) did not inhibit ADV extract-induced scratching (data not shown). Thus, our data suggest that neurogenic inflammation does not play a key role in ADV extract-induced and PAR_2-mediated scratching. It is conceivable that serine proteases from dermatophytes act directly on the pruriceptive primary afferents. However, PAR_2-immunoreactive nerve-like structures have not been observed in the skin, including the dermis just beneath the epidermis in mice (Tsujii et al., 2009). Thus, further studies are needed to elucidate the direct action of serine proteases on primary afferents.

In summary, our data suggest that serine proteases secreted by dermatophytes cause itching through activation of the PAR_2 receptors, which may be a causal mechanism of dermatophytosis itch.

Authorship Contributions

Participated in research design: Andoh, Sano, and Kuraishi.
Conducted experiments: Andoh, Takayama, and Yamakoshi.
Contributed new reagents or analytic tools: Lee and Sano.
Performed data analysis: Andoh, Takayama, Yamakoshi, Shimizu, and Kuraishi.
Wrote or contributed to the writing of the manuscript: Andoh and Kuraishi.

References

Akiyama T, Carstens MI, and Carstens E (2010) Differential itch- and pain-related behavioral responses and μ-opoid modulation in mice. *Acta Derm Venereol* **90:**575–581.

Al-Ani B, Saifeddine M, Wijesuriya SJ, and Hollenberg MD (2002) Modified proteinase-activated receptor-1 and -2 derived peptides inhibit proteinase-activated receptor-2 activation by trypsin. *J Pharmacol Exp Ther* **300:**702–708.

Andoh T and Kuraishi Y (1998) Intradermal leukotriene B_4, but not prostaglandin E_2, induces itch-associated responses in mice. *Eur J Pharmacol* **353:**93–96.

Andoh T, Katsube N, Maruyama M, and Kuraishi Y (2001) Involvement of leukotriene B_4 in substance P-induced itch-associated response in mice. *J Invest Dermatol* **117:**1621–1626.

Andoh T and Kuraishi Y (2003) Nitric oxide enhances substance P-induced itch-associated responses in mice. *Br J Pharmacol* **138:**202–208.

Andoh T, Nagasawa T, Satoh M, and Kuraishi Y (1998) Substance P induction of itch-associated response mediated by cutaneous NK_1 tachykinin receptors in mice. *J Pharmacol Exp Ther* **286:**1140–1145.

Andoh T, Nishikawa Y, Yamaguchi-Miyamoto T, Nojima H, Narumiya S, and Kuraishi Y (2007) Thromboxane A_2 induces itch-associated responses through TP receptors in the skin in mice. *J Invest Dermatol* **127:**2042–2047.

Andoh T, Saito A, and Kuraishi Y (2009) Leukotriene B_4 mediates sphingosylphosphorylcholine-induced itch-associated responses in mouse skin. *J Invest Dermatol* **129:**2854–2860.

Andoh T, Yageta Y, Takeshima H, and Kuraishi Y (2004) Intradermal nociceptin elicits itch-associated responses through leukotriene B_4 in mice. *J Invest Dermatol* **123:**196–201.

Andoh T, Zhang Q, Yamamoto T, Tayama M, Hattori M, Tanaka K, and Kuraishi Y (2010) Inhibitory effects of the methanol extract of *Ganoderma lucidum* on mosquito allergy-induced itch-associated responses in mice. *J Pharmacol Sci* **114:**292–297.

Arthur RP and Shelley WB (1955) The role of proteolytic enzymes in the production of pruritus in man. *J Invest Dermatol* **25:**341–346.

Bergasa NV, Alling DW, Talbot TL, Swain MG, Yurdaydin C, Turner ML, Schmitt JM, Walker EC, and Jones EA (1995) Effects of naloxone infusions in patients with the pruritus of cholestasis. A double-blind, randomized, controlled trial. *Ann Intern Med* **123:**161–167.

Cohen AD, Wolak A, Alkan M, Shalev R, and Vardy DA (2002) AFSS: athlete's foot severity score. A proposal and validation. *Mycoses* **45:**97–100.

Costa R, Marotta DM, Manjavachi MN, Fernandes ES, Lima-Garcia JF, Paszcuk AF, Quintão NL, Juliano L, Brain SD, and Calixto JB (2008) Evidence for the role of neurogenic inflammation components in trypsin-elicited scratching behaviour in mice. *Br J Pharmacol* **154:**1094–1103.

Djeridane A, Djeridane Y, and Ammar-Khodja A (2006) Epidemiological and aetiological study on tinea pedis and onychomycosis in Algeria. *Mycoses* **49:**190–196.

Drouot S, Mignon B, Fratti M, Roosje P, and Monod M. (2009) Pets as the main source of two zoonotic species of the *Trichophyton mentagrophytes* complex in Switzerland, *Arthroderma vanbreuseghemii* and *Arthroderma benhamiae*. *Vet Dermatol* **20:**13–18.

Fujii T, Murai M, Morimoto H, Maeda Y, Yamaoka M, Hagiwara D, Miyake H, Ikari N, and Matsuo M (1992) Pharmacological profile of a high affinity dipeptide NK1 receptor antagonist, FK888. *Br J Pharmacol* **107:**785–789.

Gotoh Y, Andoh T, and Kuraishi Y (2011) Noradrenergic regulation of itch transmission in the spinal cord mediated by á-adrenoceptors. *Neuropharmacology* **61:**825–831.

Gradisar H, Kern S, and Friedrich J (2000) Keratinase of *Doratomyces microsporus*. *Appl Microbiol Biotechnol* **53:**196–200.

Hagermark O, Rajka G, and Bergqvist U (1972) Experimental itch in human skin elicited by rat mast cell chymase. *Acta Derm Venereol* **52:**125–128.

Kuraishi Y, Nagasawa T, Hayashi K, and Satoh M (1995) Scratching behavior induced by pruritogenic but not algesiogenic agents in mice. *Eur J Pharmacol* **275:**229–233.

Kuraishi Y, Yageta Y, Konno M, Andoh T, Yamaguchi-Miyamoto T, and Nojima H (2008) Intracisternal, but not intrathecal, injection of naloxone inhibits cutaneous itch-related response in mice. *Biol Pharm Bull* **31:**2143–2145.

Macfarlane SR, Seatter MJ, Kanke T, Hunter GD, and Plevin R (2001) Proteinase-activated receptors. *Pharmacol Rev* **53:**245–282.

Maekawa T, Yamaguchi-Miyamoto T, Nojima H, and Kuraishi Y (2002) Effects of naltrexone on spontaneous itch-associated responses in NC mice with chronic dermatitis. *Jpn J Pharmacol* **90:**193–196.

Meevootisom V, and Niederpruem DJ. (1979) Control of exocellular proteases in dermatophytes and especially *Trichophyton rubrum Sabouraudia* **17:**91–106.

Miyamoto T, Nojima H, Shinkado T, Nakahashi T, and Kuraishi Y (2002) Itch-associated response induced by experimental dry skin in mice. *Jpn J Pharmacol* **88:**285–292.

Monod M (2008) Secreted proteases from dermatophytes. *Mycopathologia* **166:**285–294.

Monroe EW (1989) Efficacy and safety of nalmefene in patients with severe pruritis caused by chronic urticaria and atopic dermatitis. *J Am Acad Dermatol* **21:**135–136.

Mori S, Itoh Y, Shinohata R, Sendo T, Oishi R, and Nishibori M (2003) Nafamostat mesilate is an extremely potent inhibitor of human tryptase. *J Pharmacol Sci* **92:**420–423.

Muhsin TM and Salih TH (2001) Exocellular enzyme activity of dermatophytes and other fungi isolated from ruminants in Southern Iraq. *Mycopathologia* **150:**49–52.

Nojima H, Simons CT, Cuellar JM, Carstens MI, Moore JA, and Carstens E (2003) Opioid modulation of scratching and spinal c-fos expression evoked by intradermal serotonin. *J Neurosci* **23:**10784–10790.

Ohtsuka E, Kawai S, Ichikawa T, Nojima H, Kitagawa K, Shirai Y, Kamimura K, and Kuraishi Y (2001) Roles of mast cells and histamine in mosquito bite-induced allergic itch-associated responses in mice. *Jpn J Pharmacol* **86:**97–105.

Peres NT, Maranhão FC, Rossi A, and Martinez-Rossi NM (2010) Dermatophytes: host-pathogen interaction and antifungal resistance. *An Bras Dermatol* **85:**657–667.

Seebacher C, Bouchara JP, and Mignon B (2008) Updates on the epidemiology of dermatophyte infections. *Mycopathologia* **166:**335–352.

Shimada SG and LaMotte RH (2008) Behavioral differentiation between itch and pain in mouse. *Pain* **139:**681–687.

Shimada SG, Shimada KA, and Collins JG (2006) Scratching behavior in mice induced by the proteinase-activated receptor-2 agonist, $SLIGRL\text{-}NH_2$. *Eur J Pharmacol* **530:**281–283.

Steinhoff M, Neisius U, Ikoma A, Fartasch M, Heyer G, Skov PS, Luger TA, and Schmelz M (2003) Proteinase-activated receptor-2 mediates itch: a novel pathway for pruritus in human skin. *J Neurosci* **23:**6176–6180.

Steinhoff M, Vergnolle N, Young SH, Tognetto M, Amadesi S, Ennes HS, Trevisani M, Hollenberg MD, Wallace JL, Caughey GH, et al. (2000) Agonists of proteinase-activated receptor 2 induce inflammation by a neurogenic mechanism. *Nat Med* **6:**151–158.

Tsujii K, Andoh T, Lee JB, and Kuraishi Y (2008) Activation of proteinase-activated receptors induces itch-associated response through histamine-dependent and -independent pathways in mice. *J Pharmacol Sci* **108:**385–388.

Tsujii K, Andoh T, Ui H, Lee JB, and Kuraishi Y (2009) Involvement of tryptase and proteinase-activated receptor-2 in spontaneous itch-associated response in mice with atopy-like dermatitis. *J Pharmacol Sci* **109:**388–395.

Ui H, Andoh T, Lee JB, Nojima H, and Kuraishi Y (2006) Potent pruritogenic action of tryptase mediated by PAR-2 receptor and its involvement in anti-pruritic effect of nafamostat mesilate in mice. *Eur J Pharmacol* **530:**172–178.

Vermout S, Tabart J, Baldo A, Mathy A, Losson B, and Mignon B (2008) Pathogenesis of dermatophytosis. *Mycopathologia* **166:**267–275.

Woodfolk JA (2005) Allergy and dermatophytes. *Clin Microbiol Rev* **18:**30–43.

Yamaguchi T, Maekawa T, Nishikawa Y, Nojima H, Kaneko M, Kawakita T, Miyamoto T, and Kuraishi Y (2001) Characterization of itch-associated responses of NC mice with mite-induced chronic dermatitis. *J Dermatol Sci* **25:**20–28.

Yamaguchi T, Nagasawa T, Satoh M, and Kuraishi Y (1999) Itch-associated response induced by intradermal serotonin through $5\text{-}HT_2$ receptors in mice. *Neurosci Res* **35:**77–83.

Yu RJ, Harmon SR, and Blank F (1968) Isolation and purification of an extracellular keratinase of *Trichophyton mentagrophytes*. *J Bacteriol* **96:**1435–1436.

Zhu Y, Wang XR, Peng C, Xu JG, Liu YX, Wu L, Zhu QG, Liu JY, Li FQ, Pan YH, et al. (2009) Induction of leukotriene B_4 and prostaglandin E_2 release from keratinocytes by protease-activated receptor-2-activating peptide in ICR mice. *Int Immunopharmacol* **9:**1332–1336.

Address correspondence to: Yasushi Kuraishi, Department of Applied Pharmacology, Graduate School of Medicine and Pharmaceutical Sciences, University of Toyama, 2630 Sugitani, Toyama 930-1094, Japan. E-mail: kuraisiy@pha.u-toyama.ac.jp

Characterization of dsRNA-induced pancreatitis model reveals the regulatory role of *IFN regulatory factor 2* (*Irf2*) in *trypsinogen5* gene transcription

Hideki Hayashi[a], Tomoko Kohno[a], Kiyoshi Yasui[a], Hiroyuki Murota[b], Tohru Kimura[c], Gordon S. Duncan[d], Tomoki Nakashima[e], Kazuo Yamamoto[d], Ichiro Katayama[b], Yuhua Ma[a], Koon Jiew Chua[a], Takashi Suematsu[a], Isao Shimokawa[f], Shizuo Akira[g], Yoshinao Kubo[a], Tak Wah Mak[d,1], and Toshifumi Matsuyama[a,h,1]

[a]Division of Cytokine Signaling, Department of Molecular Biology and Immunology and [f]Department of Investigative Pathology, Nagasaki University Graduate School of Biomedical Science, Nagasaki 852-8523, Japan; Departments of [b]Dermatology and [c]Pathology, Graduate School of Medicine and [g]Department of Host Defense, Research Institute for Microbial Diseases, Osaka University, Osaka 565-0871, Japan; [d]Campbell Family Cancer Research Institute, Princess Margaret Hospital, Toronto, ON, Canada M5G 2M9; [e]Department of Cell Signaling, Tokyo Medical and Dental University, Tokyo 113-8549, Japan; and [h]Global Center of Excellence Program, Nagasaki University, Nagasaki 852-8523, Japan

Contributed by Tak Wah Mak, October 5, 2011 (sent for review September 8, 2011)

Mice deficient for *interferon regulatory factor* (*Irf*)*2* (*Irf2*$^{-/-}$ mice) exhibit immunological abnormalities and cannot survive lymphocytic choriomeningitis virus infection. The pancreas of these animals is highly inflamed, a phenotype replicated by treatment with poly(I:C), a synthetic double-stranded RNA. Trypsinogen5 mRNA was constitutively up-regulated about 1,000-fold in *Irf2*$^{-/-}$ mice compared with controls as assessed by quantitative RT-PCR. Further knockout of *IFNα/β receptor 1*(*Ifnar1*) abolished poly(I:C)-induced pancreatitis but had no effect on the constitutive up-regulation of *trypsinogen5* gene, indicating crucial type I IFN signaling to elicit the inflammation. Analysis of *Ifnar1*$^{-/-}$ mice confirmed type I IFN-dependent transcriptional activation of dsRNA-sensing pattern recognition receptor genes *MDA5*, *RIG-I*, and *TLR3*, which induced poly(I:C)-dependent cell death in acinar cells in the absence of IRF2. We speculate that Trypsin5, the *trypsinogen5* gene product, leaking from dead acinar cells triggers a chain reaction leading to lethal pancreatitis in *Irf2*$^{-/-}$ mice because it is resistant to a major endogenous trypsin inhibitor, Spink3.

TRIF | IPS-1 | Ca^{2+}-binding proteins | cathepsin B

Interferons (IFNs) are cytokines whose actions contribute to the first line of defense against infection. IFNs both render cells resistant to viral attack and regulate cell growth and differentiation (1). IFNs elicit their pleiotropic effects by regulating the expression of many IFN-stimulated genes (ISGs). IFNs themselves are controlled by IFN regulatory factors (IRFs) that also regulate the expression of ISGs. By binding to IFN-stimulated response elements (ISREs) in gene promoters, the nine known IRF family members (IRF1–9) govern the production of cytokines related to inflammation and immune responses.

When pattern recognition receptors (PRRs) such as Toll-like receptors (TLRs) and retinoic acid-inducible gene-I (RIG)-like receptors detect pathogen ligands, these receptors are activated (2) and transduce downstream signaling, activating IRFs and IFNs. Analyses using knockout (KO) mice deficient for various IRFs have revealed their physiological roles. For example, IRF2 functions mainly as a transcriptional repressor by competing for binding to ISREs with other IRFs, especially IRF9 and IRF1 (1).

Irf2-deficient (*Irf2*$^{-/-}$) mice spontaneously develop inflammatory skin disease as they age, and die within weeks from lymphocytic choriomeningitis virus (LCMV) infection (3). Ablation of *IFNα/β receptor 1* (*Ifnar1*) or *Irf9* ameliorates the skin inflammation of *Irf2*$^{-/-}$ mice, suggesting that IRF2 negatively regulates gene expression by antagonizing IRF9, which is activated by type I IFN (I-IFN) (4). However, the precise mechanisms underlying the phenotypes of *Irf2*$^{-/-}$ are not known. In this study, we found that poly(I:C) (pIC) mimicked LCMV-induced pancreatitis, and we have used double KO mice to explore the cause of death in pIC-treated *Irf2*$^{-/-}$ mice. Our results show that significant trypsinogen5 up-regulation in *Irf2*$^{-/-}$ mice together with I-IFN-dependent transcriptional activation of dsRNA-sensing PRRs were critical for the pIC-induced death.

Results and Discussion

***Irf2*$^{-/-}$ Mice Show IFN-Dependent Poly(I:C)-Induced Pancreatitis and IFN-Independent Secretory Dysfunction in Pancreatic Acinar Cells.** LCMV-infected *Irf2*$^{-/-}$ mice die within 4 wk postinfection (3), but all *Irf2*$^{-/-}$ mice challenged intraperitoneally with poly(I:C) (pIC-*Irf2*$^{-/-}$ mice) died within 1 wk (Fig. 1*A*). Severe acute pancreatitis was apparent in pIC-*Irf2*$^{-/-}$ mice, as shown by abundant TUNEL^{+} apoptotic cells (Fig. 1*B*). Even in the absence of pIC, however, some abnormalities were detected in *Irf2*$^{-/-}$ pancreas, as indicated by hematoxylin and eosin staining (Fig. 1*C*) and electron microscopy (Fig. 1*D*). A mild infiltration of inflammatory cells (particularly lymphocytes) was noted around *Irf2*$^{-/-}$ ductal cells, but this pancreatitis was not typical. The pancreatic acinar cells in untreated *Irf2*$^{-/-}$ mice were filled with eosinophilic secretory granules of heterogeneous size, whereas fewer eosinophilic granules of more uniform size were observed mainly in the apical region of WT acinar cells. Interestingly, treatment of *Irf2*$^{-/-}$ mice with the stable cholecystokinin (CCK) analog cerulein (5) did not cause acute pancreatitis, as assessed by electron microscopy and serum amylase levels (Fig. S1 *A* and *B*). Because mRNA expression of CCK receptors in *Irf2*$^{-/-}$ mice was normal (Fig. S1*C*), these results suggest that the secretory and/or vesicle transport systems in *Irf2*$^{-/-}$ mice are dysfunctional.

The mRNAs encoding the Ca^{2+}-binding proteins Anxa10, Ahsg, and S100-G involved in Ca^{2+}-dependent vesicle transport, sorting, and fusion processes were significantly up-regulated in *Irf2*$^{-/-}$ pancreas (Table S1). The secretory dysfunction observed in cerulein-treated *Irf2*$^{-/-}$ mice (6), which is due to an abnormal distribution pattern of normal levels of soluble *N*-ethylmaleimide-sensitive factor attachment protein receptors (SNAREs) (6), may be due to the abnormal expression of these Ca^{2+}-binding proteins in the absence of IRF2, because annexin family proteins are known to bind and regulate SNAREs (7).

Skin inflammation in *Irf2*$^{-/-}$ mice was rescued by abolishing IFN signaling (4). We asked whether the atypical pancreatitis in *Irf2*$^{-/-}$ mice could be similarly rescued by crossing the *Irf2*$^{-/-}$ mutants to *Ifnar1*-, *Irf1*-, or *Trif*-deficient mice (3, 8, 9) to gen-

Author contributions: H.H., T. Kohno, I.K., T.W.M., and T.M. designed research; H.H., T. Kohno, K. Yasui, H.M., T. Kimura, G.S.D., T.N., K. Yamamoto, Y.M., K.J.C., T.S., and T.M. performed research; T. Kimura, I.S., and S.A. contributed new reagents/analytic tools; Y.K. and T.W.M. analyzed data; and H.H. and T.M. wrote the paper.

The authors declare no conflict of interest.

Freely available online through the PNAS open access option.

[1]To whom correspondence may be addressed. E-mail: tmak@uhnres.utoronto.ca or tosim@nagasaki-u.ac.jp.

This article contains supporting information online at www.pnas.org/lookup/suppl/doi:10.1073/pnas.1116273108/-/DCSupplemental.

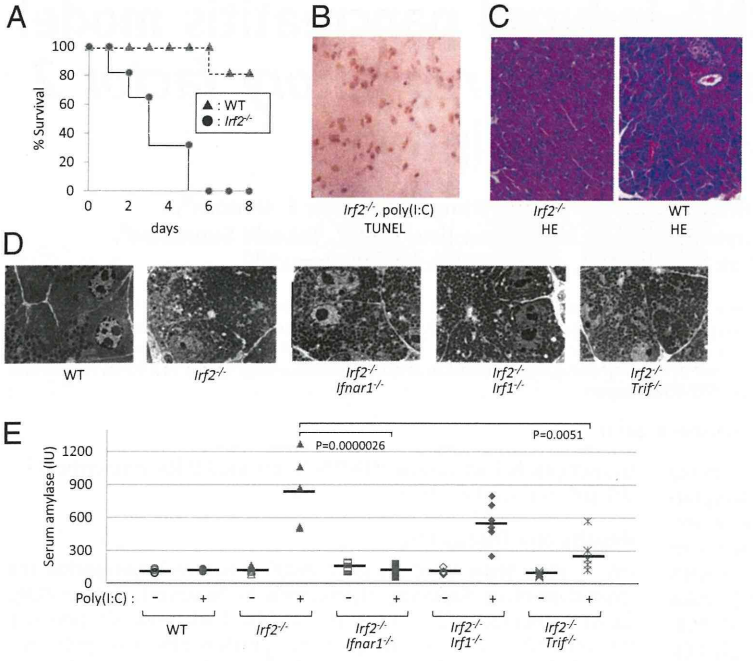

Fig. 1. *Irf2* deficiency induces sensitivity to poly(I:C) and pancreatitis. (*A*) Survival curve after pIC challenge. WT and *Irf2*-deficient ($Irf2^{-/-}$) mice were induced by i.p. pIC challenge (250 μg). All of the $Irf2^{-/-}$ mice were deceased within a week, compared with WT mice. (*B*) Following pIC stimulation, many cells were TUNEL-positive, indicating apoptosis and severe acute pancreatitis in $Irf2^{-/-}$ mice. (*C* and *D*) Hematoxylin and eosin (HE) staining (*C*) and electron microscopic observation (*D*) were done to examine the pancreas histologically in WT, $Irf2^{-/-}$, and double KO mice ($Irf2^{-/-}Ifnar1^{-/-}$, $Irf2^{-/-}Irf1^{-/-}$, and $Irf2^{-/-}Trif^{-/-}$). (*E*) To assess pancreatitis, we monitored serum amylase levels with (+) and without (–) pIC challenge.

erate double knockout mice. Abnormal acinar granule distribution was again observed in $Irf2^{-/-}Ifnar1^{-/-}$, $Irf2^{-/-}Irf1^{-/-}$, and $Irf2^{-/-}Trif^{-/-}$ mice (Fig. 1*D*). Thus, the abnormal acinar structure caused by *Irf2* disruption is not mediated by IFN signaling.

To assess pancreatitis in double knockout mice, we measured serum amylase levels before and after pIC challenge (Fig. 1*E*). Serum amylase was elevated in pIC-$Irf2^{-/-}$ and pIC-$Irf2^{-/-}Irf1^{-/-}$ mice. However, this increase did not occur at all in pIC-$Irf2^{-/-}Ifnar1^{-/-}$ mice, and only to a limited extent in pIC-IRF2$^{-/-}$TRIF$^{-/-}$ mice. These data indicate that type I IFN signaling via IFNAR1, as well as TLR signaling via the adaptor protein TRIF, are important for the development of pIC-induced pancreatitis in $Irf2^{-/-}$ mice. Moreover, our results show that IRF2 regulates IFN-independent pathways affecting acinar cell secretion as well as IFN-dependent pathways inducing pIC-mediated pancreatitis.

Up-Regulated Trypsinogen5 mRNA in the Pancreas of $Irf2^{-/-}$ Mice. We used an Affymetrix DNA microarray system to compare mRNA expression in the pancreas before and after pIC injection of $Irf2^{-/-}$ and WT mice (Fig. 2*A*). In $Irf2^{-/-}$ mice, 14 annotated genes were up-regulated and 8 genes were down-regulated more than 10-fold (Table S1) compared with WT mice. The transcriptional profiles of genes important for the etiology of pancreatitis (10, 11) are listed in Table 1. Strikingly, trypsinogen5 mRNA was up-regulated >100-fold in pIC-$Irf2^{-/-}$ pancreas, a noteworthy observation because trypsinogens activate many other pancreatic enzymes, and premature intracellular activation of trypsinogens in pancreatic acinar cells triggers acute pancreatitis (10, 11). There are 20 *trypsinogen* genes (*T1–T20*) in the murine T-cell receptor β gene locus (12), 12 of which express trypsinogen proteins (Fig. S2, *Right*), whereas humans have only 3 *trypsinogen* genes encoding three proteins: PRSS1, PRSS2, and PRSS3 (Fig. S2, *Left*) (13). The gene expression profile of pIC-$Irf2^{-/-}$ pancreas is inflammation-prone: Mouse trypsinogen mRNAs of T11 (Prss3) and T4 (Trypsinogen5) were up-regulated (Table 1); the mRNA encoding cysteine protease cathepsin B (Ctsb), an enzyme that can initiate pancreatitis by activating trypsinogens (14–16), was also up-regulated (Table 1). The mRNA encoding chymotrypsin C (Ctrc) was down-regulated and another anti-inflammatory factor inter-α-trypsin inhibitor was also down-regulated, although the mRNA encoding Kazal type 3 (Spink3), a serine protease inhibitor that blocks trypsin activity (17), was slightly up-regulated.

We examined the tissue specificity and dependency on IRF2 and IFNAR1 of trypsinogen5 expression by quantitative RT-PCR. In untreated WT mice, trypsinogen5 is expressed most highly in pancreas and skin and modestly in spleen (Fig. S3*A*). In untreated $Irf2^{-/-}$ mice, trypsinogen5 expression in the pancreas was up-regulated ~1,000-fold compared with controls, and was not affected by IFNAR1 ablation. Trypsinogen5 mRNA was up-regulated in $Irf2^{-/-}$ spleen to a much lower extent than in $Irf2^{-/-}$ pancreas, and was not detectable in liver or lung of WT or $Irf2^{-/-}$ mice.

We examined the effects of various IRFs on the activity of the murine *trypsinogen5* promoter, which contains seven ISREs. We cloned a 1.1-kb fragment of the *trypsinogen5* promoter region (−1063 to +15) to create a series of promoter deletion construct mutants driving the firefly luciferase reporter gene (Fig. 2*B*, *Left*). These were transfected into HEK293T cells along with plasmids overexpressing murine IRF1, human IRF5, IRF7, or MyD88. MyD88 was required for IRF-mediated activation of *trypsinogen5* ISREs, and significant promoter activity was observed when IRF1, IRF5, or IRF7 was overexpressed (Fig. S3*B*). Furthermore, the −216 to +15 promoter region of *trypsinogen5* was sufficient for responses to IRF1 or IRF7 stimulation (Fig. S3*C*). Overexpression of IRF2 inhibited IRF1- or IRF7-stimulated promoter activity in a dose-dependent manner (Fig. S3*D*). These data suggest that IRF2 binds to the proximal promoter of *trypsinogen5* and inhibits the access of IRF1, IRF5, and IRF7 to ISRE sites in this region.

To confirm this hypothesis, we transfected TGP49 cells, a mouse acinar cell line, with *trypsinogen5* promoter deletion series reporters as well as with plasmids expressing IRF1, -5, or -7, and assessed the promoter activities (Fig. 2*B*, *Right*). The basal promoter activity was drastically decreased by deleting the −216 to −100 region containing two ISREs, a nuclear factor-activated T cell (NFAT), and an activator protein 1 (AP-1) binding site. In contrast to 293T cells, the *trypsinogen5* promoter in TGP49 cells could be activated by exogenously expressed IRF5 or IRF7 without MyD88 (Fig. 3*A*). The promoter could not be activated by IRF1 even in the presence of MyD88 expression. The regions responsive to IRF5 and IRF7 were confirmed to be ISRE4 (−62 to −59) and ISRE3 (−55 to −49) by site-specific mutation analysis (Fig. 2*C*). The IRF5- and IRF7-dependent promoter activities were significantly ($P < 0.05$) enhanced by knocking down Irf2 with specific siRNA compared with control (scrambled) siRNA (Fig. 3*A*).

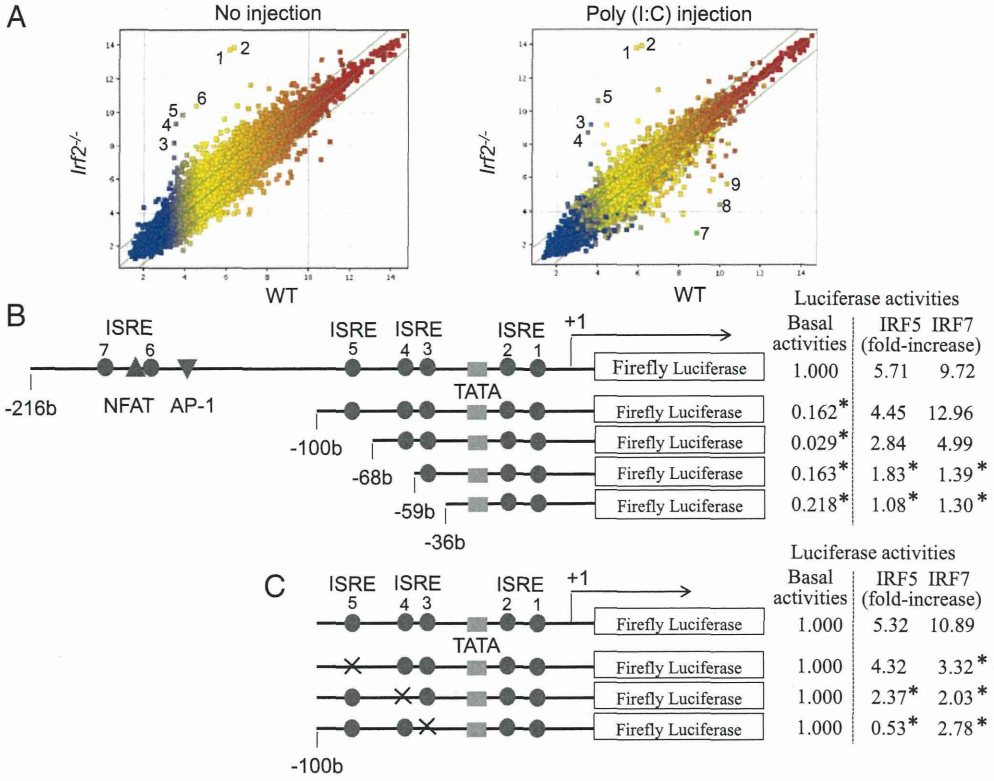

Fig. 2. Trypsinogen5 is highly expressed in *Irf2*-deficent mice. (*A*) *Irf2*$^{-/-}$ or wild-type mice with or without peritoneal injection of pIC were killed, and the amounts of mRNA from the pancreas were systematically compared using Affymetrix 28,815 gene probes. The points farthest from the diagonal indicate transcripts showing the greatest difference between WT and *Irf2*$^{-/-}$. Points 1 and 2, trypsinogen5 with different probes; 3, α-2-HS-glycoprotein (Ahsg); 4, annexin A10 (Anxa10); 5, fetuin-β (Fetub); 6, 3-hydroxy-3-methylglutaryl-CoenzymeA synthase2 (Hmgcs2, HMG-CoA synthase); 7, Ig κ chain variable8 (Igk-V8); 8, unknown; 9, carbonic anhydrase 3 (Car3). (*B*) A series of deletion mutants of *trypsinogen5* proximal promoter region (−216 to +15) was placed upstream of a luciferase reporter gene (1 μg) and analyzed for transcriptional activity in mouse pancreatic acinar cells using a dual luciferase assay at 24 h posttransfection in combination with expression vectors (100 ng) expressing IRF5 or IRF7 or a control vector. The basal luciferase activity of each deletion, measured relative to the −216 to +15 region, and the responses to IRF5 and IRF7 expression vectors are shown as fold increase compared with the control vector. The TATA box, ISRE core, and NFAT- and AP-1 binding sites are indicated. *$P < 0.05$ versus the −216 to +15 region. (*C*) Point mutations were introduced into each ISRE site (indicated by x) of the *trypsinogen5* promoters as described in *Materials and Methods*. The promoter activity of each mutant *trypsinogen5* was determined with a dual luciferase assay system. *$P < 0.05$ versus wild type.

To confirm IRF2 binding to the proximal promoter of trypsinogen5 in pancreatic acinar cells in vivo, we performed chromatin immunoprecipitation (ChIP) assays in TGP49 cells using specific PCR probes spanning all seven ISREs (−173 to +56) in the *trypsinogen5* promoter. Anti-IRF2 antibody specifically precipitated the *trypsinogen5* promoter, as determined by semi-quantitative PCR (Fig. 3*B*) and real-time PCR (Fig. 3*C*). These results suggest that in WT mice, trypsinogen5 expression in pancreatic acinar cells is repressed by the binding of IRF2 to ISREs in the proximal promoter region. However, in *Irf2*$^{-/-}$ mice, the *trypsinogen5* gene is activated because IRF5 and IRF7 can access the ISREs in the absence of IRF2.

IRF5 and IRF7 are critical inducers of the expression of proinflammatory cytokines and type I IFNs, respectively (18, 19), and these activities require MyD88. In WT cells, IRF4 inhibits IRF5 function by sequestering MyD88 (18). IRF2 did not associate with MyD88 (18) but, in our study, it did bind to the ISRE-containing region in the trypsinogen5 promoter (Fig. 3 *B* and *C*). Therefore, we postulate that IRF2 inhibits IRF5 and IRF7 activity by competing with them for binding to ISREs, rather than by sequestering MyD88.

Trypsinogen5 Is Resistant to the Trypsin Inhibitor Spink3. Comparison of mouse trypsinogen5 to other mouse and human trypsinogens (Fig. S4) showed that, although the N-terminal activation peptide sequence (NSDDK-I) in trypsinogen5 differs from that in other trypsinogens (DDDDK-I), other important regions, including the triad amino acid sequence H-D-S, required for enzymatic activity are conserved (10, 11). In addition, tryptic activity in cell lysates of 293FT cells overexpressing trypsinogen5 was dramatically enhanced by treatment with enteropeptidase (Fig. 4 *A* and *B*). The trypsinogen5 inhibitor binding site (DSCDGDS), which prevents premature activation, differed from that found in most trypsinogens (DSCQGDS) (10, 11), resembling the inhibitor binding site (DSCQRDS) of the human trypsin inhibitor-resistant PRSS3 enzyme. In addition, the trypsin autolytic cleavage site (Q-V) in trypsinogen5 differed from that in other trypsinogens (R-V), suggesting that trypsinogen5 is resistant to both trypsin inhibitors and self-inactivation. Indeed, trypsinogen5 was resistant to inhibition by Spink3, a major en-

Table 1. Expressions of relevant genes to pancreatitis

Gene transcripts	WT (−)	WT (pIC)	*Irf2*$^{-/-}$ (−)	*Irf2*$^{-/-}$ (pIC)
Prss1 (T16, Trypsin1)	11,161	13,863	10,388	13,788
Prss2 (T20, Trypsin 2)	16,041	15,661	15,857	15,494
Prss3 (T11, Trypsin 3)	1,155	1,131	3,059 ↑	2,395 ↑
Trypsinogen5 (T4, 1810009J06Rik)	70	57	13,514 ↑	14,287 ↑
Chymotrypsin C (Ctrc)	545	368	87 ↓	119 ↓
Chymotrypsinogen B 1 (Ctrb1)	19,417	18,772	20,457	19,919
Amylase2-2, pancreatic (Amy2b)	19,101	18,488	17,092	18,261
Calcium-sensing receptor (Casr)	37	37	30	26
Cystic fibrosis membrane conductance regulator (Cftr)	7	6	11	8
Cathepsin B (Ctsb)	349	443	848 ↑	794 ↑
Serine protease inhibitor, Kazal-type 3 (Spink3)	4,716	3,957	7,497	7,774
Inter-α-trypsin inhibitor, heavy chain 4 (Itih4)	375	212	78 ↓	71 ↓
Galanin (Gal)	879	1,057	213 ↓	71 ↓

The levels of gene expression in the pancreas are shown in Affymetrix units. The trypsinogen5 data are Point 1 in Fig. 2.

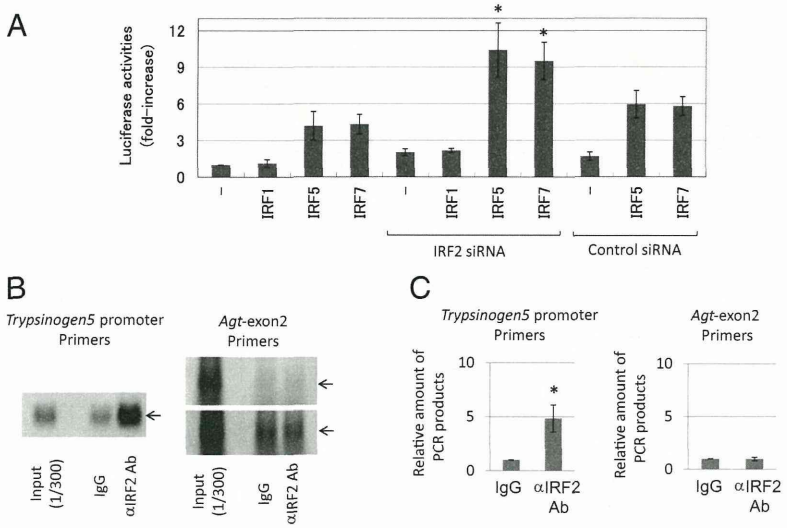

Fig. 3. IRF2 binds to the promoter region of *trypsinogen5* gene. (*A*) The effects of siRNAs (3 μg) specific to IRF2 or a control scrambled sequence on transcriptional activity of the −216 to +15 luciferase reporter in TGP49 acinar cells were measured. $*P < 0.05$ versus control siRNA. (*B*) A chromatin immunoprecipitation assay was done using TGP49 acinar cells with the IRF2-specific antibody (5 μg) or the same amount of control nonspecific IgG. The precipitated chromatin fragments were detected by PCR with a *trypsinogen5* promoter-specific primer set at 35 cycles or a negative control primer set for *angiotensinogen* (*Agt*) exon2 at 30 (*Upper*) and 35 (*Lower*) cycles. The input before precipitation indicates the predicted size (Trp5, 229 bp; Agt, 221 bp) of the PCR product. (*C*) The ChIP assay done in *B* was quantitatively measured using a real-time PCR method with the same primers. The relative amounts of β-actin were calculated, and the amounts of chromatin fragments precipitated with the anti-IRF2 antibody were shown relative to those with the nonspecific control antibody (IgG). $*P < 0.01$ versus control IgG.

dogenous trypsin inhibitor in mice (Fig. 4 *C* and *D*), as well as by soy bean trypsin inhibitor (Fig. S5 *A* and *B*). Analysis of the evolutionary pedigree in Fig. S6 showed that mouse trypsinogen5 is most distant from mPrss1 and mPrss2, just as human PRSS3 is most distant from PRSS1 and PRSS2. Therefore, we believe that mouse trypsinogen5 is a homolog of human PRSS3. Moreover, our data suggest that, in the absence of IRF2, trypsinogen5 is highly expressed and exacerbates pIC-induced pancreatitis due to its inhibitor-resistant nature.

Poly(I:C)-Induced Cell Death Can Be Triggered by a TLR3/TRIF-Dependent Pathway or a RIG-I/MDA5/IPS-1-Dependent Pathway. Although trypsinogen5 was up-regulated in untreated IRF2$^{-/-}$ mice, only mild inflammation around acinar cells was observed and pancreatitis did not occur. We hypothesize that trypsinogen5 as well as mPrss1, -2, and -3 leaking from dying acinar cells are activated by proteases such as cathepsin B or enteropeptidase, also released from these cells. These activated trypsins trigger signals to induce the death of many acinar cells, a process of cell death amplification we refer to as the "enhancing loop" of acinar cell death. In this way, the initial death of a few cells induced by pIC can precipitate severe pancreatitis. This idea is supported by a report that the extracellular or intracellular treatment of pancreatic acinar cells with active trypsins causes acinar cell death (20). In this study, the enteropeptidase cleavage site (-DDDDK-) of rat trypsinogen was replaced with a cleavage site (-RTKR-) recognized by paired basic amino acid-cleaving enzyme (PACE). This allowed the rat trypsinogen to be activated intracellularly with the ubiquitously expressed PACE enzyme rather than with enteropeptidase, which is expressed mainly in the duodenum. We created a PACE-trypsinogen5 enzyme that successfully induced the apoptosis of 293FT cells when overexpressed (Fig. 4 *E* and *F*). These results indicate that proteolytic activation of trypsinogen5 is sufficient to induce cell death.

Because pIC-dependent pancreatitis in *Irf2*$^{-/-}$ mice can be prevented by inactivating IFNAR1 signaling (Fig. 1*E*), we focused on IFN signaling pathways to identify candidates that might trigger initial cell death following pIC treatment. Indeed,

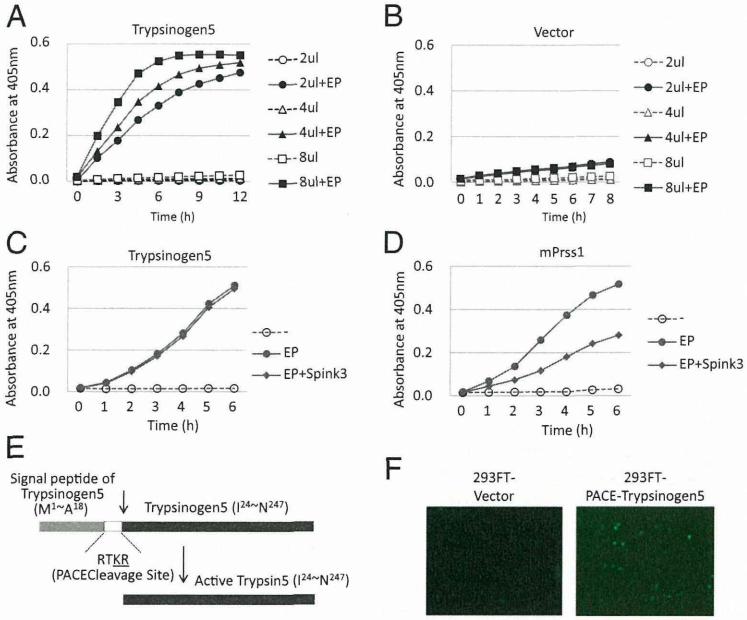

Fig. 4. Trypsinogen activity is activated by proteolytic cleavage. (*A* and *B*) A full-length mouse trypsinogen5 cDNA from the mouse pancreas was cloned into pcDNA3 (Invitrogen) and expressed in 293T cells. The indicated amounts of cell lysates (2–8 μL of 5 μg/μL lysates) were mixed with a trypsin-specific substrate (BioVision) in the presence or absence of added enteropeptidase. Tryptic activity was monitored by the amount of released pNA, measuring spectrophotometric units (A_{405}). (*C* and *D*) The effects of Spink3 were examined by adding cell lysates expressing Spink3, a major intrinsic trypsin inhibitor in mouse pancreas, to lysates expressing trypsinogen5 (*C*) or mouse Prss1 (*D*). (*E*) The DNA sequence encoding the activation peptide in the trypsinogen5 expression vector was replaced with sequences encoding a PACE cleavage site (-RTKR-) so that tryptic activity is activated by ubiquitously expressed PACE protease. (*F*) 293FT cells transfected with PACE-trypsinogen5 or control vector were stained with FITC-labeled annexin V to detect apoptosis.

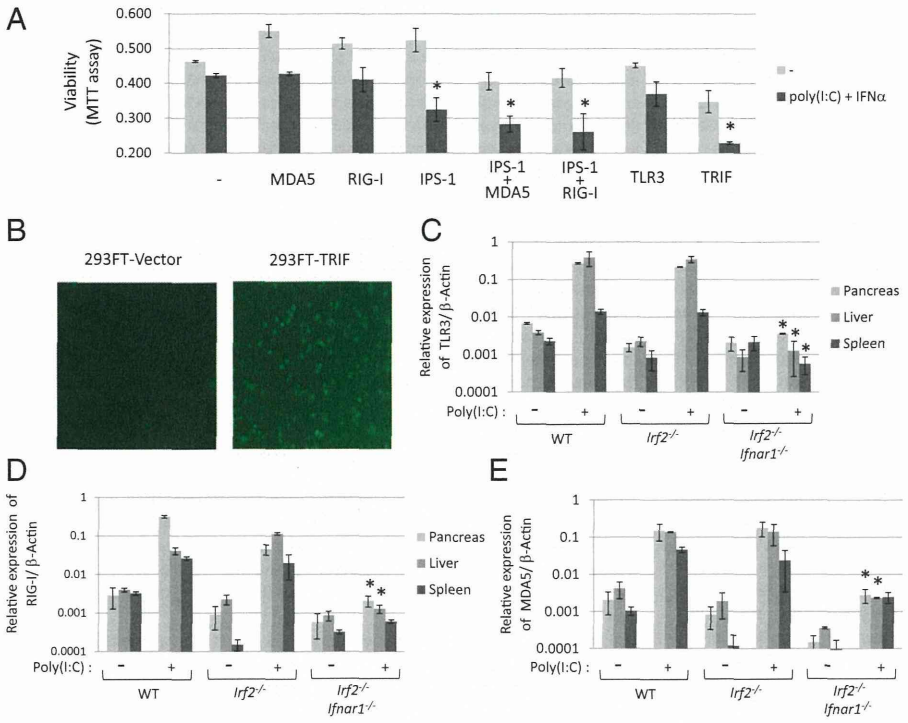

Fig. 5. Poly(I:C) and IFNα treatment induces cell death through different pathways. (*A*) Viabilities of 293FT cells transfected with the indicated expression plasmids in the presence or absence of pIC (5 μg/mL) and IFNα (50 ng/mL) for 44 h were quantified with the MTT assay. The values represent the average of at least three separate experiments, with SDs shown by error bars. TRIF and IPS-1 with MDA5 or RIG-I induced significant (*$P < 0.02$) cell death in response to pIC and IFNα. (*B*) 293FT cells transfected with TRIF expression vector or vector alone were stained with FITC-labeled annexin V to detect apoptosis. mRNA expression levels of TLR3 (*C*), RIG-I (*D*), and MDA5 (*E*) were measured using real-time PCR with (+) or without (–) i.p. pIC injection (250 μg). mRNAs prepared from pancreas, liver, and spleen of WT, *Irf2*$^{-/-}$, and *Irf2*$^{-/-}$*Ifnar1*$^{-/-}$ mice were converted into cDNA, and the amount of cDNA was determined by real-time PCR with the specific primers listed in *SI Materials and Methods*. The values represent the average of at least two mice, with SDs shown by error bars. *$P < 0.05$ versus *Irf2*$^{-/-}$ mice.

IRF1, *IRF7*, *MyD88*, *MDA5*, *RIG-I*, and *TLR3* gene expression were all up-regulated in the pancreas of pIC-*Irf2*$^{-/-}$ mice (Table S2). Because these proteins are associated with cell death pathways dependent on TRIF or IPS-1, we examined the effect of IRF2 loss on these well-characterized systems (21, 22). TRIF binds to receptor-interacting proteins and thereby activates caspase8 via FADD to induce cell death (21), whereas the IPS-1-dependent cell death pathway, which is triggered by MDA5 or RIG-I, is reported to activate caspase9 via the mitochondrial pathway dependent on Apaf-1 and cytochrome *c* (22). We confirmed that 293FT cells transfected with TRIF-expressing plasmid underwent apoptosis, as shown by staining with FITC-labeled annexin V (Fig. 5*B*). Next, we used the MTT viability assay to quantify the extent of cell death induced by IFN-related molecules in the presence or absence of pIC and IFNα. Exogenous overexpression of IPS-1 or TRIF significantly enhanced the death of pIC- and IFN-treated 293FT cells, and the death-inducing effects of MDA5 and RIG-I were enhanced by cotransfection with IPS-1 (Fig. 5*A*). These results suggest the existence of at least two pIC-dependent cell death pathways: one TLR3/TRIF-dependent and one RIG-I/MDA5/IPS-1-dependent.

We used real-time PCR to examine the induction of TLR3, RIG-I, and MDA5 mRNAs in pIC-treated WT, *Irf2*$^{-/-}$, and *Irf2*$^{-/-}$*Ifnar1*$^{-/-}$ mice. The levels of all three mRNAs were induced by nearly 100-fold in both pIC-WT and pIC-*Irf2*$^{-/-}$ mice, and these increases were abolished by deletion of IFNAR1 (Fig. 5 *C–E*). The IFN signal activation triggered by pIC is essential to initiate TLR3/TRIF- and RIG-I/MDA5/IPS-1-dependent acinar cell death, but is not sufficient to cause pancreatitis (Table S3). The elevation of trypsinogen5 expression mediated by abolishing IRF2 is also necessary for enhancing the cell death leading to lethal pancreatitis.

Activation Mechanisms of Mouse Trypsinogen5 and Human PRSS3. Trypsinogens (including trypsinogen5) can be activated in pancreatic acinar cells, or in other cells or tissues by enteropeptidase expressed in nonduodenal cells (23) such as in keratinocytes and oral carcinoma cells (24, 25). It is possible that keratinocyte-expressed enteropeptidase activates the trypsinogen5 expressed in skin (Fig. S3*A*), promoting age-dependent skin inflammation in *Irf2*$^{-/-}$ mice (4). Another possibility could be that proteases in addition to enteropeptidase can cleave pancreatic trypsinogen5. We have confirmed that cathepsin B, whose expression was elevated in *Irf2*$^{-/-}$ mice, can activate trypsinogen5 in vitro (Fig. S5*C*). The last possibility is that autocatalytic cleavage of trypsinogen, usually restricted under steady-state conditions, is accelerated in response to chemical stress or viral infection. Indeed, the autoactivation of trypsinogen is reportedly accelerated in low pH or by Ca^{2+} in vitro (26).

In conclusion, this study has identified important genes associated with IRF2 functions in mice. Our results suggest that IRF2 influences the expression of mouse trypsinogen5, whose human counterpart is PRSS3. Our data should therefore help to elucidate new IRF functions in humans.

Materials and Methods

Mice. *Irf1*$^{-/-}$ and *Irf2*$^{-/-}$ mice have been described (3). *IFNαlβ receptor 1* (*Ifnar1*)$^{-/-}$ mice were purchased from B&K Universal (8). TRIF$^{-/-}$ mice have been described (9). *Irf2*$^{-/-}$*Ifnar1*$^{-/-}$, *Irf2*$^{-/-}$*Irf1*$^{-/-}$, and *Irf2*$^{-/-}$*Trif*$^{-/-}$ double mutant mice were generated by crossing *Irf2*$^{+/-}$ with *Ifnar1*$^{-/-}$, *Irf1*$^{-/-}$, and *Trif*$^{-/-}$ mice, respectively. All mice were maintained under specific pathogen-free conditions and used at 6–12 wk of age. All experiments were performed according to institutional guidelines.

Cells. Human embryonic kidney (HEK)293T and 293FT (Invitrogen) cells and HeLa cells were cultured in DMEM supplemented with 10% FBS. Mouse pancreatic acinar TGP49 cells were cultured in a 1:1 mixture of DMEM and Ham's F-12 medium supplemented with 10% FBS.

Histological Analysis. Pancreas tissues were fixed overnight in 10% formalin, embedded in paraffin, sectioned, and stained with hematoxylin (0.4%) and eosin (0.5%) for light microscopic analysis. For electron microscopic analysis, the tissues were fixed in 2.5% glutaraldehyde solution buffered to pH 7.4 with 0.1 M phosphate buffer for 4 h at 4 °C. Postfixation was performed with 2% osmium tetroxide solution buffered to pH 7.4 with the same buffer for 2 h at 4 °C, and they were embedded, sectioned, and doubly stained with uranyl acetate and lead nitrate.

Microarrays. Total RNAs from the pancreas of wild-type and *Irf2*$^{-/-}$ mice aged 6 wk, harvested 3 h after no injection or a peritoneal injection with 250 μg poly(I:C), were used in the array studies. The quality of the RNA was assessed with an Agilent 2100 Bioanalyzer, and samples of 100 ng total RNA were reverse-transcribed and then amplified by in vitro transcription according to Affymetrix standard protocols. The mouse Affymetrix GeneChip Mouse Gene 1.0 ST Array was used in all hybridizations. These arrays contain probes representing transcripts for 28,815 mouse gene entities. Microarray data were analyzed using Affymetrix Expression Console software and Gene Spring GX, whereas differentially expressed genes were identified with annotation.

Real-Time RT-PCR. Total RNA was prepared from tissues using the acid phenol-guanidinium thiocyanate method after immersing the tissues for more than overnight in RNAlater Solution (Ambion). Reverse transcription was conducted for 60 min at 46 °C from 200 ng of purified total RNA using SuperScript III (Invitrogen), followed by 45 cycles of PCR (15-s denaturation at 95 °C, 25-s annealing at 55 °C, and 15-s extension at 72 °C). An SYBR Green PCR Kit (Qiagen) was used to monitor the PCR products on a LightCycler 1.5 and real-time PCR detection system (Roche). Primers designed for the respective genes are listed in *SI Materials and Methods*.

Plasmid Constructs. cDNAs encoding human IRF5, IRF7, and IPS-1 were generated from total RNA prepared from 293T cells by RT-PCR using KOD-FX DNA polymerase (Toyobo). Human MDA5, RIG-I, and TLR3 cDNAs were generated from total RNA prepared from THP-1 (a human leukemia cell line) or HeLa cells by RT-PCR. Mouse Trypsinogen5, Prss1, and Spink3 cDNAs were made from total RNA prepared from WT mouse pancreas by PCR. All constructs generated by PCR were confirmed by DNA sequencing. The p*Trypsinogen5*-Luc reporter plasmid was constructed by inserting the promoter region (−1063 to +15) of the mouse *trypsinogen5* gene by PCR into the pGL2-Basic vector. A series of deletion mutants was prepared using proper restriction enzymes (NcoI at −833; SpeI at −579; ScaI at −386; PvuII at −216) and a specific primer for the −100 site. The promoter region (−216 to +15) of the mouse *trypsinogen5* gene was used to introduce point mutations into the ISREs. The point mutations of ISRE3 (−55 to −49, ATTGAAA→GTTTGCG), ISRE4 (−62 to −59, TTTC→CGCA), and ISRE5 (−84 to −78, AATGAAA→GATTGCG) were introduced by overlap PCR mutagenesis. All constructs generated by PCR were confirmed by DNA sequencing.

PACE-Trypsinogen5 was constructed by replacing the activation peptide (-NSDDK-) of mouse trypsinogen5 cDNA with the PACE recognition peptide (-RTKR-) by overlap PCR mutagenesis.

Luciferase Reporter Assay. 293T cells (1×10^5 per well) were plated in 24-well plates and transfected 24 h later with 200 ng of the firefly luciferase reporter plasmid p*Trypsinogen5*-Luc, using FuGENE6 (Roche), along with each expression vector (20 ng unless otherwise stated) as indicated. In all cases, cells were transfected with 20 ng pRL-TK (*thymidine kinase* promoter-driven Renilla luciferase reporter gene; Promega) to normalize the transfection efficiency. TGP49 cells (1×10^5 per well) were plated in 12-well plates and transfected 24 h later with 1 μg of the firefly luciferase reporter plasmid pTrypsinogen5-Luc using Lipofectamine 2000 (Invitrogen), along with each expression vector (100 ng unless otherwise stated) as indicated. In all cases, cells were transfected with 20 ng pRL-RSV (RSV promoter-driven Renilla luciferase reporter gene). At 26 h posttransfection, luciferase activity was determined with a dual luciferase assay system (Promega). Mouse IRF2-specific and control siRNAs were purchased from Santa Cruz Biotechnology.

Chromatin Immunoprecipitation. Nuclear extracts from TGP49 cells were subjected to DNA–protein cross-linking with 1% formaldehyde for 5 min. After extensive washing, the samples were suspended in 500 μL of 150 mM NaCl, 25 mM Tris (pH 7.5), 5 mM EDTA, 1% Triton X-100, 0.1% SDS, and 0.5% deoxycholate and sonicated. After centrifugation at 14,000 rpm for 10 min at 4 °C, the supernatants were immunoprecipitated with 0.5 μg anti-IRF2 antibody, or the corresponding IgG (Sigma) (as a control), and Protein A Sepharose4B Fast Flow beads. The amounts of precipitated DNA were quantified by PCR using a pair of mouse *Trypsinogen5* promoter-specific primers and *Angiotensinogen* exon2-specific primers (*SI Materials and Methods*).

Trypsin Activity Assay. Trypsin activity was monitored by the amount of released *p*-nitroanilide (pNA) from a specific substrate, measuring spectrophotometric units at 405 nm (A_{405}) (Trypsin Activity Assay Kit; BioVision). Cell lysates prepared at 48 h posttransfection of the indicated expression plasmids were used with or without enteropeptidase (light chain, porcine; GenScript).

Cell Death Assay. Pancreatic tissues were used in a TUNEL assay. Briefly, tissue sections were incubated with 20 μg/mL proteinase K for 20 min, followed by inhibition of endogenous peroxidase by incubation with 2% H_2O_2 for 7 min. TdT (GIBCO-BRL) and biotinylated dUTP (Roche) in TdT buffer [0.1 M potassium cacodylate (pH 7.2), 2 mM $CoCl_2$, 0.2 mM DTT] were added to the sections and incubated in a humid atmosphere at 37 °C for 90 min after immersion in TdT buffer. The reaction was terminated by transferring the slides to TB buffer (300 mM NaCl, 30 mM Na citrate) for 30 min. The sections were covered with 10% rabbit serum for 10 min and then with the avidin–biotin peroxidase complex for 30 min. Finally, 3,3′-diaminobenzidine (DAB) was used as the chromogen. To detect apoptotic cells, FITC-conjugated annexin V (BioVision) was used according to the manufacturer's instruction. An MTT (ICN) assay to assess living cells was performed according to the manufacturer's instruction.

ACKNOWLEDGMENTS. This work was supported by Grants-in-Aid from the Ministry of Education, Culture, Sports, Science and Technology of Japan (22659092) and by the Global Center of Excellence Program at Nagasaki University.

1. Savitsky D, Tamura T, Yanai H, Taniguchi T (2010) Regulation of immunity and oncogenesis by the IRF transcription factor family. *Cancer Immunol Immunother* 59:489–510.
2. Kawai T, Akira S (2011) Toll-like receptors and their crosstalk with other innate receptors in infection and immunity. *Immunity* 34:637–650.
3. Matsuyama T, et al. (1993) Targeted disruption of IRF-1 or IRF-2 results in abnormal type I IFN gene induction and aberrant lymphocyte development. *Cell* 75:83–97.
4. Hida S, et al. (2000) CD8(+) T cell-mediated skin disease in mice lacking IRF-2, the transcriptional attenuator of interferon-α/β signaling. *Immunity* 13:643–655.
5. Lampel M, Kern H-F (1977) Acute interstitial pancreatitis in the rat induced by excessive doses of a pancreatic secretagogue. *Virchows Arch A Pathol Anat Histol* 373:97–117.
6. Mashima H, et al. (2011) Interferon regulatory factor-2 regulates exocytosis mechanisms mediated by SNAREs in pancreatic acinar cells. *Gastroenterology* 141:1102–1113.
7. Gerke V, Creutz C-E, Moss S-E (2005) Annexins: Linking Ca^{2+} signalling to membrane dynamics. *Nat Rev Mol Cell Biol* 6:449–461.
8. Hwang SY, et al. (1995) A null mutation in the gene encoding a type I interferon receptor component eliminates antiproliferative and antiviral responses to interferons α and β and alters macrophage responses. *Proc Natl Acad Sci USA* 92:11284–11288.
9. Yamamoto M, et al. (2003) Role of adaptor TRIF in the MyD88-independent Toll-like receptor signaling pathway. *Science* 301:640–643.
10. Chen J-M, Férec C (2009) Chronic pancreatitis: Genetics and pathogenesis. *Annu Rev Genomics Hum Genet* 10:63–87.
11. Whitcomb D-C (2010) Genetic aspects of pancreatitis. *Annu Rev Med* 61:413–424.
12. Spicuglia S, Pekowska A, Zacarias-Cabeza J, Ferrier P (2010) Epigenetic control of Tcrb gene rearrangement. *Semin Immunol* 22:330–336.
13. Rowen L, et al. (2005) Interchromosomal segmental duplications explain the unusual structure of PRSS3, the gene for an inhibitor-resistant trypsinogen. *Mol Biol Evol* 22:1712–1720.
14. Figarella C, Miszczuk-Jamska B, Barrett A-J (1988) Possible lysosomal activation of pancreatic zymogens. Activation of both human trypsinogens by cathepsin B and spontaneous acid. Activation of human trypsinogen 1. *Biol Chem Hoppe Seyler* 369 (Suppl):293–298.
15. Halangk W, et al. (2000) Role of cathepsin B in intracellular trypsinogen activation and the onset of acute pancreatitis. *J Clin Invest* 106:773–781.
16. Meister T, et al. (2010) Missorting of cathepsin B into the secretory compartment of CI-MPR/IGFII-deficient mice does not induce spontaneous trypsinogen activation but leads to enhanced trypsin activity during experimental pancreatitis—without affecting disease severity. *J Physiol Pharmacol* 61:565–575.
17. Hashimoto D, et al. (2008) Involvement of autophagy in trypsinogen activation within the pancreatic acinar cells. *J Cell Biol* 181:1065–1072.
18. Negishi H, et al. (2005) Negative regulation of Toll-like-receptor signaling by IRF-4. *Proc Natl Acad Sci USA* 102:15989–15994.
19. Honda K, et al. (2005) Spatiotemporal regulation of MyD88-IRF-7 signalling for robust type-I interferon induction. *Nature* 434:1035–1040.
20. Ji B, Gaiser S, Chen X, Ernst S-A, Logsdon C-D (2009) Intracellular trypsin induces pancreatic acinar cell death but not NF-&kappaB activation. *J Biol Chem* 284: 17488–17498.
21. Kaiser W-J, Offermann M-K (2005) Apoptosis induced by the Toll-like receptor adaptor TRIF is dependent on its receptor interacting protein homotypic interaction motif. *J Immunol* 174:4942–4952.
22. Lei Y, et al. (2009) MAVS-mediated apoptosis and its inhibition by viral proteins. *PLoS One* 4:e5466.
23. Yahagi N, et al. (1996) Complementary DNA cloning and sequencing of rat enteropeptidase and tissue distribution of its mRNA. *Biochem Biophys Res Commun* 219:806–812.
24. Nakanishi J, Yamamoto M, Koyama J, Sato J, Hibino T (2010) Keratinocytes synthesize enteropeptidase and multiple forms of trypsinogen during terminal differentiation. *J Invest Dermatol* 130:944–952.
25. Vilen S-T, et al. (2008) Intracellular co-localization of trypsin-2 and matrix metalloprotease-9: Possible proteolytic cascade of trypsin-2, MMP-9 and enterokinase in carcinoma. *Exp Cell Res* 314:914–926.
26. Chen J-M, et al. (2003) Evolution of trypsinogen activation peptides. *Mol Biol Evol* 20: 1767–1777.

blood

2012 120: 76-85
Prepublished online May 18, 2012;
doi:10.1182/blood-2011-12-399113

Critical role of P1-Runx1 in mouse basophil development

Kaori Mukai, Maya J. BenBarak, Masashi Tachibana, Keigo Nishida, Hajime Karasuyama, Ichiro Taniuchi and Stephen J. Galli

Blood (print ISSN 0006-4971, online ISSN 1528-0020), is published weekly by the American Society of Hematology, 2021 L St, NW, Suite 900, Washington DC 20036.

Critical role of P1-Runx1 in mouse basophil development

Kaori Mukai,[1,2] Maya J. BenBarak,[1] Masashi Tachibana,[3] Keigo Nishida,[4] Hajime Karasuyama,[2] Ichiro Taniuchi,[3] and Stephen J. Galli[1]

[1]Department of Pathology, Stanford University School of Medicine, Stanford, CA; [2]Department of Immune Regulation, Japan Science and Technology Agency, Core Research for Evolutionary Science and Technology, Tokyo Medical and Dental University Graduate School, Tokyo, Japan; and [3]Laboratory for Transcriptional Regulation and [4]Laboratory for Cytokine Signaling, RIKEN Research Center for Allergy and Immunology, Kanagawa, Japan

$Runx1^{P1N/P1N}$ mice are deficient in the transcription factor distal promoter-derived Runt-related transcription factor 1 (P1-Runx1) and have a > 90% reduction in the numbers of basophils in the BM, spleen, and blood. In contrast, $Runx1^{P1N/P1N}$ mice have normal numbers of the other granulocytes (neutrophils and eosinophils). Although basophils and mast cells share some common features, $Runx1^{P1N/P1N}$ mice have normal numbers of mast cells in multiple tissues. $Runx1^{P1N/P1N}$ mice fail to develop a basophil-dependent reaction, IgE-mediated chronic allergic inflammation of the skin, but respond normally when tested for IgE- and mast cell–dependent passive cutaneous anaphylaxis in vivo or IgE-dependent mast cell degranulation in vitro. These results demonstrate that $Runx1^{P1N/P1N}$ mice exhibit markedly impaired function of basophils, but not mast cells. Infection with the parasite *Strongyloides venezuelensis* and injections of IL-3, each of which induces marked basophilia in wild-type mice, also induce modest expansions of the very small populations of basophils in $Runx1^{P1N/P1N}$ mice. Finally, $Runx1^{P1N/P1N}$ mice have normal numbers of the granulocyte progenitor cells, SN-Flk2$^{+/-}$, which can give rise to all granulocytes, but exhibit a > 95% reduction in basophil progenitors. The results of the present study suggest that P1-Runx1 is critical for a stage of basophil development between SN-Flk2$^{+/-}$ cells and basophil progenitors. (*Blood.* 2012;120(1):76-85)

Introduction

Basophils are the least prevalent of the granulocytes, generally representing less than 1% of leukocytes in the peripheral blood. Basophil studies have been hampered by the rarity of these cells and, until recently, the lack of tools such as basophil-deficient mice with which to assess their roles in vivo. However, recent studies have unveiled evidence for several previously unrecognized roles for basophils that are distinct from those of mast cells.[1-11]

In addition to hampering investigations of basophil function, the small numbers of basophils and the paucity of tools for their analysis have made studies of basophil development challenging and therefore there have been few studies of this process. Arinobu et al showed that basophil lineage-restricted progenitors (BaPs) are identifiable in the BM and that the transcription factor CCAAT/enhancer-binding protein-α (C/EBPα) is important for the fate decision to develop into terminally differentiated basophils.[12] Ohmori et al reported that the IL-3–STAT5 axis is important for differentiating granulocyte-monocyte progenitors to BaPs,[13] and Siracusa et al showed that thymic stromal lymphopoietin (TSLP) can facilitate the development of BaPs into mature basophils.[8]

Despite such progress, many of the details of the basophil differentiation pathway remain to be determined. For example, it is known that IL-3–deficient,[8,14,15] TSLP receptor (TSLPR)–deficient,[8] and IL-3/TSLPR double-deficient[8] mice have normal baseline numbers of basophils, indicating that other factors are more important in maintaining basophil levels at baseline. Moreover, C/EBPα-deficient mice die within 8 hours of birth[16] and STAT5-deficient mice die in utero,[17] limiting the ability to use these animals to evaluate factors that might regulate basophil development at baseline in adult mice in vivo.

Runt-related transcription factor (Runx) proteins are a family of transcription factors[18,19] that have crucial roles during the development of many tissues and the immune system. Each of the 3 kinds of Runx proteins, Runx1, Runx2, and Runx3,[19,20] has distinct roles in development, with Runx1 being required for hematopoiesis,[18] Runx2 for osteogenesis,[21,22] and Runx3 for neurogenesis, thymopoiesis, and the control of gastric epithelial-cell proliferation.[23-25] Although a constitutive deficiency in Runx1 is embryonically lethal, studies of conditional Runx1-knockout mice have indicated that Runx1 can regulate the differentiation of hematopoietic stem cells (HSCs), B lymphocytes, natural killer T (NKT) cells, and T lymphocytes.[18,26-30] Mx-Cre Runx1-knockout mice, which have an inducible Runx1 inactivation system, exhibit normal numbers of HSCs, a normal myeloid-cell (neutrophil) compartment, a severe reduction in megakaryocyte differentiation and platelet formation, and defects in B and T lymphocytes.[31] All 3 Runx genes can be transcribed from the distal (P1) or proximal (P2) promoters,[32] and P1- and P2-derived Runx1 variants differ in their N-terminal end sequences. It has been reported previously that variation in the expression of P1- versus P2-Runx1 can be regulated developmentally, but it remains to be elucidated how such Runx1 variants influence the development of different types of immune cells.[33]

We report herein evidence indicating that P1-derived Runx1 is important for basophil development in mice at baseline. P1-Runx1–deficient mice have a drastic reduction (more than 90%) in

Submitted December 16, 2011; accepted May 5, 2012. Prepublished online as *Blood* First Edition paper, May 18, 2012; DOI 10.1182/blood-2011-12-399113.

The online version of this article contains a data supplement.

The publication costs of this article were defrayed in part by page charge payment. Therefore, and solely to indicate this fact, this article is hereby marked "advertisement" in accordance with 18 USC section 1734.

basophils but normal numbers of the other granulocytes (neutrophils and eosinophils) and normal numbers of mast cells in multiple anatomic sites. The results of the present study strongly suggest that, in mice, P1-Runx1 is an important regulator of the differentiation of basophils, but not other granulocytes, and plays a nonredundant role in basophil, but not mast cell, development.

Methods

Mice

Runx1$^{P1N/P1N}$ mice, which have been described previously,[34] were backcrossed onto a C57BL/6 background (8-10 generations, 6-12 weeks of age). We mated *Runx1*$^{P1N/+}$ mice and *Runx1*$^{P1N/+}$ mice in our animal facility to obtain *Runx1*$^{P1N/P1N}$ mice and littermate *Runx1*$^{+/+}$ wild-type (WT) control mice. All animal care and experimentation was conducted according to the guidelines of RIKEN, Stanford University, and the National Institutes of Health with the specific approval of the institutional animal care and use committee of Stanford University.

Abs, flow cytometry, and cell culture

The Abs used for cytometry were from BD Pharmingen, eBiosciences, or BioLegend. For analysis of lineage cells, we used mIgE-biotin (R35-72), CD49b-Alexa Fluor 488 (DX5), Gr-1–FITC (RB6-8C5), Siglec-F–PE (E50-2440), NK-1.1-APC (PK136), B220-APC (RA3-6B2), CD11c-FITC (HL3), c-Kit–APC (2B8), FcεRIα-PE (MAR-1), CD3-FITC (145-2C11), CD4-FITC (L3T4), CD8-APC (53-6.7), and CD11b-FITC (M1/70). Surface staining was performed for 15-20 minutes with the corresponding mixture of fluorescently labeled Abs. Data were acquired on a FACSCalibur flow cytometer or FACSAria II cell sorter (BD Biosciences) and analyzed with FlowJo Version 8.8.6 software (TreeStar). The cell sorting technique used has been described previously.[35] Briefly, BM cells were depleted for the lineage markers CD3 (145-2C11), CD4 (L3T4), CD5 (53-7.3), CD8 (53-6.7), B220 (RA3-6B2), Gr-1 (RB6-8C5), CD11b (M1/70), and Ter119 (Ter-119) by MACS LD columns with anti–rat IgG microbeads (Miltenyi Biotec). SN progenitors were sorted on a FACSAria II cell sorter using the labeled mAbs Pacific Blue–conjugated CD3 (145-2C11), CD4 (L3T4), CD8 (53-6.7), CD11b (M1/70), Ter119 (Ter-119), Gr-1 (RB6-8C5), Sca-1–PE/Cy5.5 (D7), β7-integrin–PE (M293), c-Kit–APC-eFlour780 (2B8), CD150-PE/Cy5 (TC15-12F12.2), Ly6C-FITC, FcεRIα-FITC (MAR-1), CD71-FITC (RI7217), CD41-FITC (MWReg30), CD27-APC (LG.3A10), and Flk2-biotin (A2F10). BaPs were sorted on a FACSAria II using the following labeled mAbs: FITC-conjugated CD4 (L3T4), CD8 (53-6.7), Gr-1 (RB6-8C5), CD11b, B220, CD11c, FcεRIα-PE (MAR-1), CD34-eFlour660 (RAM34), and c-Kit–APC-eFlour780 (2B8). Basophil mast cell bipotential progenitors (BMCPs) were sorted on a FACSAria II using the following labeled mAbs: Pacific Blue–conjugated CD3 (145-2C11), CD4 (L3T4), CD8 (53-6.7), CD11b (M1/70), Ter119 (Ter-119), Gr-1 (RB6-8C5), β7-integrin–PE (M293), c-Kit–APC (2B8), and PE-Cy7–FcγR.93 Single cells were sorted using a FACSAria II into 96-well round-bottom plates containing growth medium (IMDM) supplemented with 20% FCS and IL-3 (30 ng/mL), IL-5 (20 ng/mL), IL-6 (10 ng/mL), GM-CSF (20 ng/mL), and SCF (20 ng/mL). All cytokines were purchased from PeproTech. After 7 days in culture at 37°C, half of each well was removed from culture and the remaining half was supplemented with fresh medium and growth factors. The half that was removed was split into 2 parts: half was analyzed by flow cytometry on a LSRFortessa (BD Biosciences) and the other half was used for cytospin followed by anti–mMCP-8 staining[36] and May-Grunwald-Giemsa staining as described previously[35,36]; we performed those analyses again after an additional 4 days of culture. For some BMCP cultures, in addition to the culture medium described above (containing 5 cytokines), we used medium containing 10 cytokines, namely, IMDM supplemented with 20% FCS with SCF (20 ng/mL), IL-3 (20 ng/mL), IL-5 (50 ng/mL), IL-6 (20 ng/mL), IL-7 (20 ng/mL), IL-9 (50 ng/mL), IL-11 (10 ng/mL), GM-CSF (10 ng/mL), erythropoietin (2 units/mL), and thrombopoietin (10 ng/mL; R&D Systems), as described by Arinobu et al.[12]

Semiquantitative RT-PCR analysis

Total RNA was prepared from total BM cells and then subjected to first-strand cDNA synthesis with RT using oligo-dT primers. Semiquantitative PCR was performed with 3-fold serially diluted cDNA templates. The primers were described previously.[36]

IgE-mediated chronic allergic skin inflammation

IgE-mediated chronic allergic skin inflammation was elicited as described previously.[37] Briefly, mice were passively sensitized with IgE by an IV injection of 300 μg of trinitrophenol (TNP)–specific IgE (IGELb4).[38] The next day, 10 μg of TNP11-conjugated ovalbumin (OVA; Biosearch Technologies) in 10 μL of PBS was injected intradermally into the left ear pinna of the mice under light anesthesia, and an equal amount of OVA was injected into the right ear pinna using a microsyringe. Ear thickness was measured with a dial thickness gauge (G1-A; Oazki) at the indicated time points. The difference in ear thickness was calculated at each time point.

Passive cutaneous anaphylaxis

Mice were sensitized passively with an intradermal injection of 2 μg of DNP-specific IgE (SPE-7; Sigma-Aldrich) in 20 μL of PBS into the right ear pinna. As a control, the same volume of PBS was injected into the left ear pinna. The mice were challenged 24 hours later with an IV injection of 250 μg of DNP_{30}-BSA (LSL) plus 1.25 mg of Evans blue dye (Sigma-Aldrich) in 250 μL of PBS. Thirty minutes after antigen challenge, the mice were euthanized, and the Evans blue dye was extracted from each dissected ear pinna in 500 μL of acetone/water (7:3) at 37°C overnight. The Evans blue in the extracts was measured with a spectrophotometer at 620 nm and calculated based on the standard.

BMCMC degranulation assay

For the BM-derived cultured mast cell (BMCMC) assay, cells were sensitized with 1 μg/mL an anti-DNP IgE mAb (SPE-7 or ε-26[39]) for 12 hours at 37°C. After sensitization, the cells were washed twice with Tyrode buffer (10mM HEPES, pH 7.4, 130mM NaCl, 5mM KCl, 1.4mM $CaCl_2$, 1mM $MgCl_2$, and 5.6mM glucose), suspended in the same buffer containing 0.1% BSA, and stimulated with polyvalent dinitrophenyl-human serum albumin (DNP_{23}-HAS; Biosearch Technologies) at 0, 6.25, 12.5, 25, 50, and 100 ng/mL for 30 minutes. For the β-hexosaminidase reaction, 50 μL of supernatant or cell lysate and 100 μL of 1.3 mg/mL p-nitrophenyl-N-acetyl-D-glucosamide (in 0.1M citrate, pH 4.5) were added to each well of a 96-well plate, and the color was developed for 60 minutes at 37°C. The enzyme reaction was then stopped by adding 150 μL of 0.2M glycine-NaOH, pH 10.2, and the absorbance at 405 nm was measured in a microplate reader (Bio-Rad). Cells were lysed with Tyrode buffer containing 1% Triton X-100 and the β-hexosaminidase activity was measured. The percentage of β-hexosaminidase released was calculated using the following formula: release (%) = supernatant/(supernatant + cell lysate) × 100.

Histologic analysis

Ear, back skin, and stomach specimens were fixed with 10% formalin and embedded in paraffin. Then, 4-μm sections were stained with 0.1% Toluidine blue for histologic examination of mast cells. Mast cells were quantified according to area (per square millimeter) for ear and back skin and per linear millimeter of tissue for glandular stomach and forestomach. Images were captured with an Olympus BX60 microscope using a Retiga-2000R QImaging camera run by Image-Pro Plus Version 6.3 software (Media Cybernetics).

ELISA

BMCMCs from WT or *Runx1*$^{P1N/P1N}$ mice were sensitized with an anti-DNP IgE mAb[39] overnight and then stimulated with 10 ng/mL of DNP_{23}-HSA (Biosearch Technologies) for 16 hours. ELISA for IL-6 was performed using an ELISA kit from BD Biosciences.

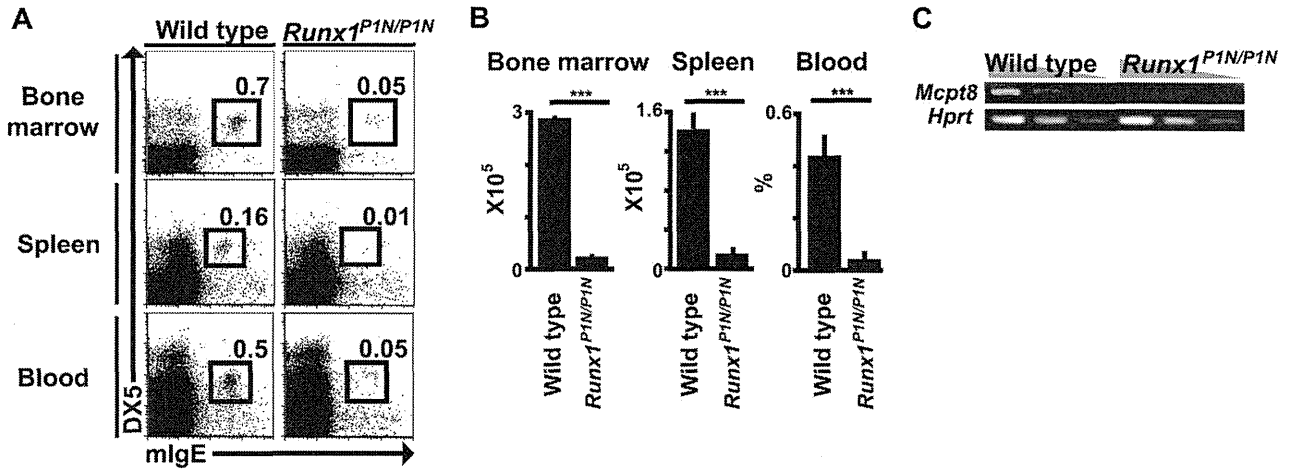

Figure 1. *Runx1*$^{P1N/P1N}$ mice have markedly reduced numbers of basophils. (A) BM, spleen, and blood were isolated from WT and *Runx1*$^{P1N/P1N}$ mice and stained with anti-IgE and anti-DX5 mAbs. Data shown are representative of 5 independent experiments, each of which gave similar results. (B) The numbers of basophils are shown as means + SEM. ***$P < .0001$; no asterisks, $P > .05$. (C) Semiquantitative RT-PCR analysis for *Mcpt8*, which encodes mMCP-8, was performed using RNA prepared from total BM cells from WT or *Runx1*$^{P1N/P1N}$ mice. cDNA was diluted 3-fold. Data shown are from 1 of 3 independent experiments, each of which gave similar results.

Nematode infection

WT or *Runx1*$^{P1N/P1N}$ mice were infected with 10 000 *Strongyloides venezuelensis* L3 larvae. BM and spleen were analyzed 8 days after infection.

Treatment with cytokines in vivo

WT or *Runx1*$^{P1N/P1N}$ mice were treated with daily IP injections of IL-3 (200 ng/d; PeproTech) for 7 consecutive days, TSLP (400 ng/d; R&D Systems) for 5 consecutive days, or vehicle (PBS) for 7 or 5 consecutive days. Basophils in the BM and spleen were analyzed the day after the 7th day (for IL-3 vs PBS) or 5th day (for TSLP vs PBS) injection. The IL-3 complex (IL-3 10 μg plus anti–IL-3 Ab 10 μg; MP2-8F8; BD Biosciences) was prepared as described previously[13] and mice were analyzed 3 days after a single IV injection.

Results

Basophils are severely reduced in *Runx1*$^{P1N/P1N}$ mice

To investigate the roles of the P1-Runx1 variant protein in vivo, we recently established mice in which the N-terminal sequences for P1-Runx1 were replaced with neo^r gene (*Runx1*^{P1N} allele), resulting in the absence of both P1-Runx1 transcripts and protein.[34] We had demonstrated previously a requirement for P1-Runx1 in lymphoid tissue inducer cell differentiation,[40] and found that *Runx1*$^{P1N/P1N}$ mice have severe reductions in NKT cells, mild T-cell deficits, and an increase in Lin$^-$c-Kit$^+$Sca-1$^+$ HSCs.[40] However, there have been no previous reports describing the myeloid cell compartment in these mice. When we analyzed myeloid cells in *Runx1*$^{P1N/P1N}$ mice, we found that they have a severe reduction in basophils. Compared with corresponding WT mice, *Runx1*$^{P1N/P1N}$ mice have a greater than 90% reduction of basophils in the BM, spleen, and blood (Figure 1A-B). To examine this phenotype using a different approach, we performed RT-PCR for *Mcpt8*, which encodes the basophil-associated marker, mouse mast cell protease 8.[36] Under the RT-PCR conditions used, *Mcpt8* mRNA was not detectable in total BM cells of *Runx1*$^{P1N/P1N}$ mice, but was readily detected in corresponding samples from WT mice (Figure 1C). These results provided additional evidence of the drastic reduction in basophils in *Runx1*$^{P1N/P1N}$ mice.

Normal numbers of eosinophils, neutrophils, and mast cells in *Runx1*$^{P1N/P1N}$ mice

There are 3 types of granulocytes: neutrophils, eosinophils, and basophils. Because *Runx1*$^{P1N/P1N}$ mice virtually lack basophils, we analyzed numbers of the other granulocytes in the mutant mice. Neutrophils (Gr-1^{high}Siglec-F$^-$) and eosinophils (Gr-1^{low}Siglec-F$^+$) were detected by flow cytometry at normal numbers in both the BM and spleen of *Runx1*$^{P1N/P1N}$ mice compared with WT mice (Figure 2A-B). In addition to these granulocytes, numbers of monocytes (Gr-1^{low}Siglec-F$^-$), NK cells (NK1.1$^+$CD3$^-$), total T cells (CD3$^+$), B cells (B220$^+$), and dendritic cells (CD11c$^+$) were not significantly different in *Runx1*$^{P1N/P1N}$ mice compared with WT mice in either the BM or spleen (Figure 2A-B). As we reported previously,[40] NKT cells (NK1.1$^+$CD3$^+$) were reduced in both the BM and spleen (Figure 2A-B). These data indicate that, among granulocyte populations, basophils are uniquely deficient in *Runx1*$^{P1N/P1N}$ mice.

Basophils are often compared with mast cells because they share certain features such as the expression of the high-affinity IgE receptor (FcεRIα) and the ability to secrete, after the appropriate stimulation, a similar (although distinct) spectrum of mediators, including histamine, lipid mediators, and cytokines.[2,41] To examine whether there is also a deficit in mast cells in these mutant mice, we quantified numbers of mast cells in several tissues. Compared with normal WT mice, *Runx1*$^{P1N/P1N}$ mice exhibited no differences in the numbers of mast cells in the peritoneal cavity (Figure 3A), ear or back skin, glandular stomach, or forestomach (Figure 3B). These findings reveal that, unlike basophils, the mast cell populations analyzed are not dependent on P1-Runx1 to achieve normal numbers at baseline.

Basophil, but not mast cell, function is abolished in *Runx1*$^{P1N/P1N}$ mice

Although *Runx1*$^{P1N/P1N}$ mice have normal numbers of mast cells (as shown in Figure 3), we wished to examine the function of mast cells in *Runx1*$^{P1N/P1N}$ mice. It is well known that the development of IgE-dependent passive cutaneous anaphylaxis requires mast cells.[42] We injected the ear pinnae of WT mice and *Runx1*$^{P1N/P1N}$ mice with a DNP-specific IgE mAb or with PBS as a control, and then

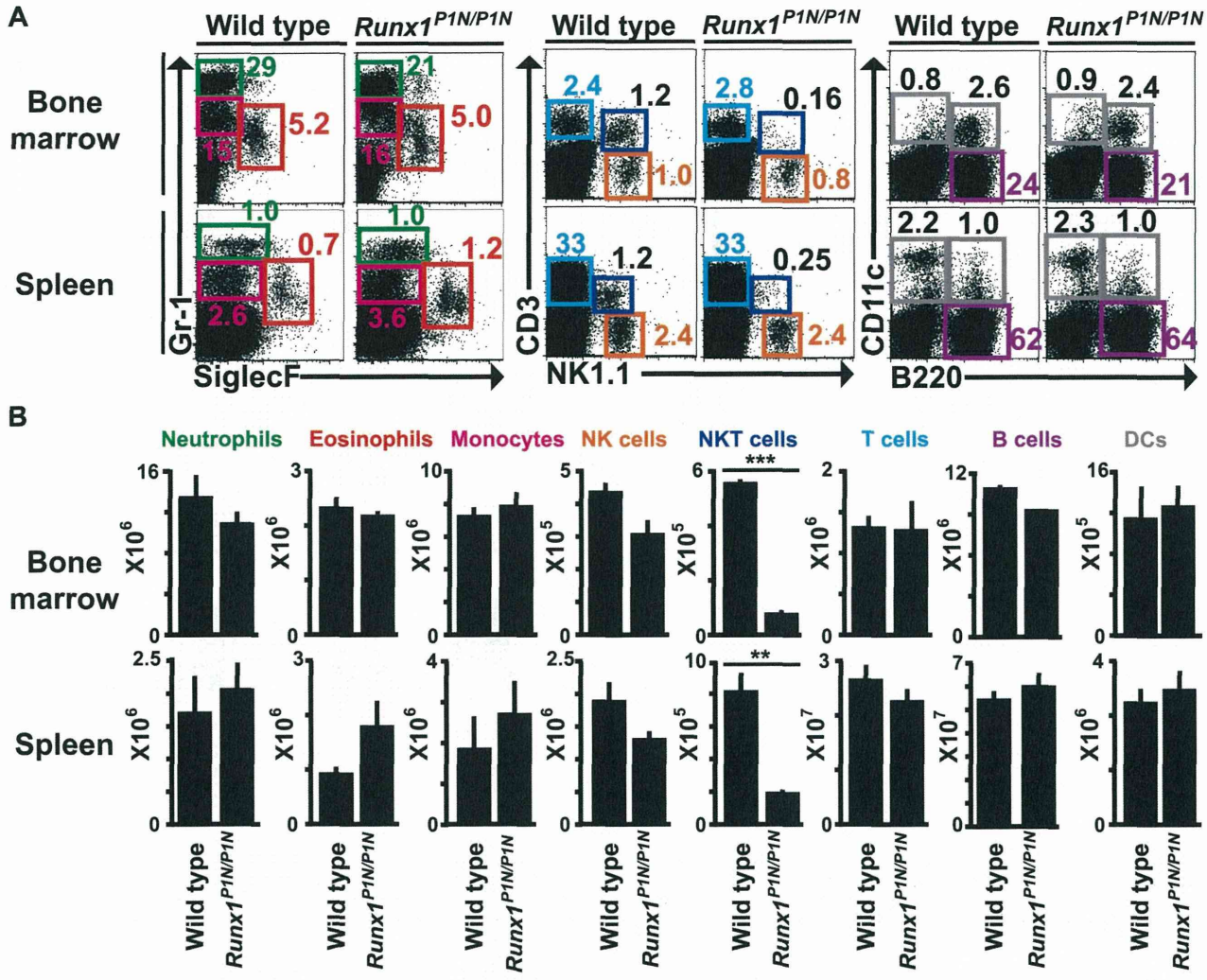

Figure 2. Phenotypic analysis of other granulocytes and leukocytes in *Runx1*$^{P1N/P1N}$ mice. (A) Representative flow cytometric plots of neutrophils (Gr-1^{high} SiglecF$^-$), eosinophils (Gr-1^{int} SiglecF$^+$), monocytes (Gr-1^{int} SiglecF$^-$), NK cells (NK1.1$^+$CD3$^-$), NKT cells (NK1.1$^+$CD3$^+$), B cells (B220$^+$), conventional dendritic cells (DCs; CD11c$^+$B220$^-$), plasmacytoid dendritic cells (CD11c$^+$B220$^+$), and T cells (CD3$^+$), and their cell counts (B) from BM and spleens from WT or *Runx1*$^{P1N/P1N}$ mice. Data shown are from 1 of 3 independent experiments, each of which gave similar results. Data in panel B show means + SEM.

challenged them intravenously the next day with antigen (DNP-BSA) plus Evans blue. Thirty minutes after antigen challenge, the mice were killed, the ears were dissected, and Evans blue was extracted. There were no significant differences in the amount of extracted dye at IgE- or PBS-injected sites between WT and *Runx1*$^{P1N/P1N}$ mice (Figure 4A).

We also tested mast cells from WT or *Runx1*$^{P1N/P1N}$ mice in vitro. We found no differences in the numbers or rate of development of BM-derived cultured mast cells (BMCMCs; > 99% c-Kit$^+$FcεRIα^+ by flow cytometry) from WT versus *Runx1*$^{P1N/P1N}$ mouse BM cells maintained as usual in IL-3–containing medium (data not shown). BMCMCs were sensitized with a DNP-specific IgE mAb overnight, then washed, and stimulated with DNP-HSA. Degranulation was quantified by measuring β-hexosaminidase release. BMCMCs from WT versus *Runx1*$^{P1N/P1N}$ mice exhibited similar levels of degranulation (Figure 4B) and IL-6 production (Figure 4C) after challenge with IgE and specific antigen. These results detected no abnormality in IgE-dependent function in *Runx1*$^{P1N/P1N}$ mast cells.

Although it is well known that IgE-mediated immediate type reactions are mast cell–dependent, Mukai et al reported that a type of IgE-mediated chronic skin reaction (IgE-dependent chronic allergic inflammation of the skin [IgE-CAI]) is dependent on basophils but not mast cells.[37] We therefore tested whether *Runx1*$^{P1N/P1N}$ mice exhibited attenuation or absence of this basophil-dependent biologic response. WT mice and *Runx1*$^{P1N/P1N}$ mice were sensitized intravenously with a TNP-specific IgE mAb and challenged intradermally the next day with the corresponding antigen (TNP-OVA) or the control carrier protein (OVA). We found that the tissue swelling associated with the IgE-CAI response was essentially eliminated in *Runx1*$^{P1N/P1N}$ mice (Figure 5A). Histologic analysis of TNP-OVA–challenged ear pinnae on day 4 showed marked infiltrates of leukocytes, including basophils (cells stained with anti–mMCP-8 Ab, which were observed in high numbers in the specimens from WT but not *Runx1*$^{P1N/P1N}$ mice; Figure 5B). Flow cytometric analysis confirmed that there were few infiltrating myeloid cells in the TNP-OVA–challenged ear pinnae of *Runx1*$^{P1N/P1N}$ vs WT mice (supplemental Figure 1A-B, available on the *Blood* Web site; see the Supplemental Materials link at the top of the online article). In addition, levels of mRNA for IL-4 and mMCP-8 were up-regulated in the TNP-OVA–challenged ear pinnae of WT but not *Runx1*$^{P1N/P1N}$ mice (supplemental Figure 1C). These results confirm previously reported results[43] indicating that basophils play a pivotal role in eliciting myeloid cell infiltration of the dermis in

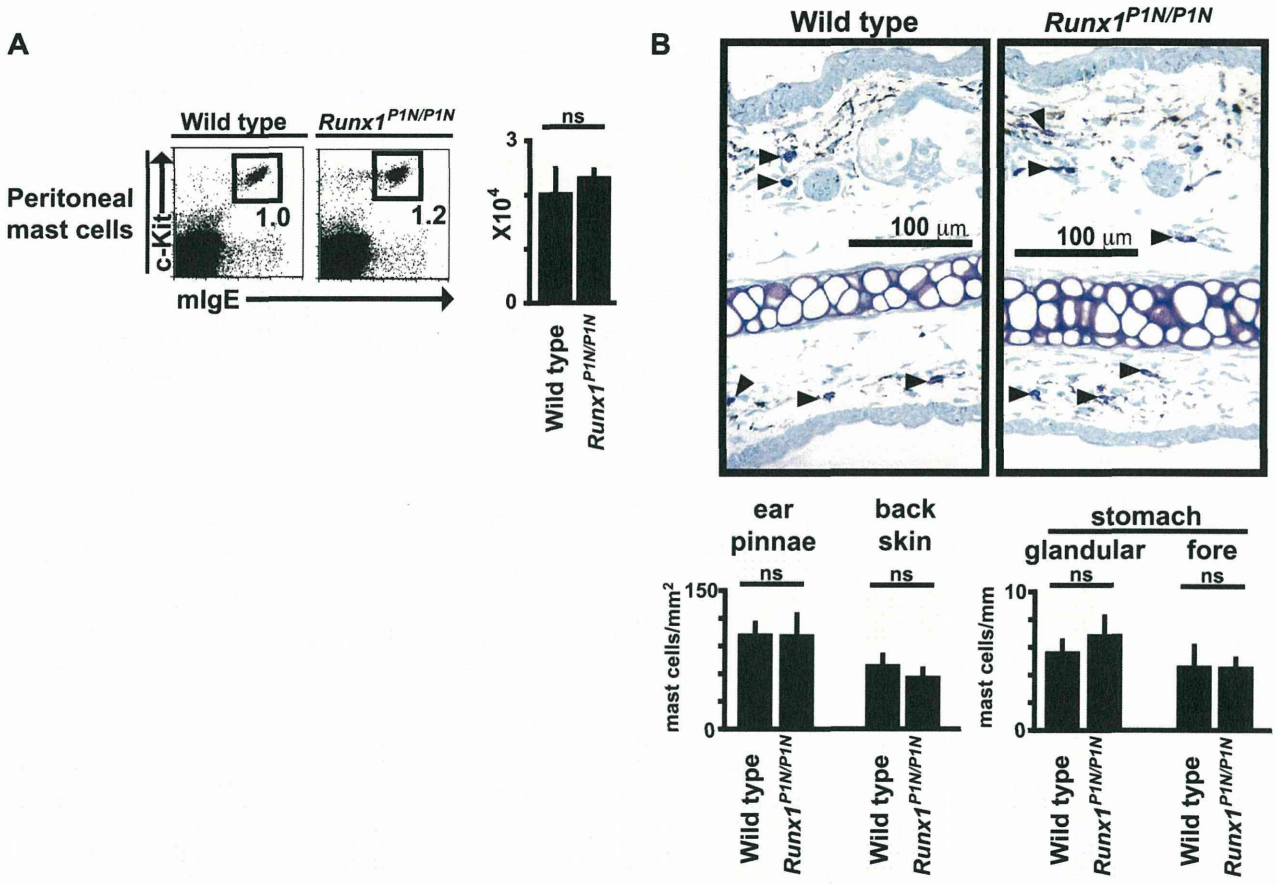

Figure 3. *Runx1*$^{P1N/P1N}$ mice have normal numbers of mast cells in multiple anatomic sites. (A) Cells from peritoneal lavage fluid were stained with anti-mIgE and anti–c-Kit mAbs. Data shown are from 1 of 5 independent experiments, each of which gave similar results. The numbers of peritoneal mast cells are shown as means + SD. ns indicates not significant ($P > .05$). (B) Toluidine blue staining for mast cells (some indicated by solid arrows) in 4-mm-thick paraffin sections of ear pinnae from WT (top) and *Runx1*$^{P1N/P1N}$ mice (bottom). The numbers of mast cells in the ear pinnae, back skin, or stomach are shown as means + SD. ns indicates not significant ($P > .05$).

IgE-CAI responses, and show that the basophil deficiency observed in *Runx1*$^{P1N/P1N}$ mice is sufficient to result in a marked reduction in the basophil-dependent IgE-CAI response.

Taken together, our results show that *Runx1*$^{P1N/P1N}$ mice exhibit a marked deficiency in a basophil-dependent immune response (as well as a marked deficiency in basophil numbers) but appear to exhibit normal levels of the IgE-dependent mast cell functions analyzed.

Nematode infection or IL-3 injection fail to induce marked basophilia in *Runx1*$^{P1N/P1N}$ mice

It has been reported that basophil numbers expand during infection with certain nematodes.[14,15,44] To investigate this in *Runx1*$^{P1N/P1N}$ mice, WT or mutant mice were infected by subcutaneous inoculation with 10 000 *S venezuelensis* third-stage infective larvae. Eight days after *S venezuelensis* infection, we analyzed

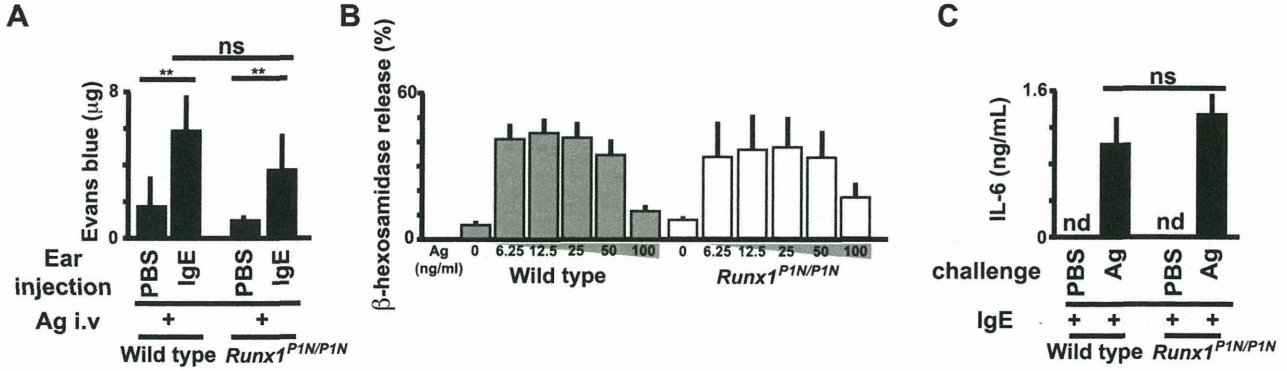

Figure 4. *Runx1*$^{P1N/P1N}$ mice have normal mast-cell functions. (A) Analysis of passive cutaneous anaphylaxis reactions in WT and *Runx1*$^{P1N/P1N}$ mice that received intradermal injections of IgE anti-DNP into the right ear pinnae and of saline into the left ear pinnae (control; none). After sensitization, mice were challenged intravenously with DNP-BSA. Data show means + SD of the extravasation of Evans blue into the ears. (B) Degranulation of WT and *Runx1*$^{P1N/P1N}$ BMCMCs, assessed as the release of β-hexosaminidase. BMCMCs were sensitized with anti-DNP IgE and stimulated with the indicated concentrations of DNP-HSA (0, 6.25, 12.5, 25, 50, and 100 ng/mL). Data show the means + SD. (C) ELISA of IL-6 in BMCMCs from WT and *Runx1*$^{P1N/P1N}$ mice sensitized with anti-DNP IgE and stimulated with DNP-HSA (10 ng/mL). nd indicates not detected. $***P < .0001$; $**P < .001$; no asterisks, $P > .05$ relative to the corresponding WT mice. Data are from 1 of 3 independent experiments, each of which gave similar results.